NRL Report 8796

Comparison of Six Integrators Used in Long-Term Radar Integrations

BEN H. CANTRELL

Radar Analysis Branch
Radar Division

April 6, 1984

NAVAL RESEARCH LABORATORY
Washington, D.C.

SECURITY CLASSIFICATION OF THIS PAGE

REPORT DOCUMENTATION PAGE

1a. REPORT SECURITY CLASSIFICATION UNCLASSIFIED	1b. RESTRICTIVE MARKINGS
2a. SECURITY CLASSIFICATION AUTHORITY	3. DISTRIBUTION/AVAILABILITY OF REPORT Approved for public release; distribution unlimited.
2b. DECLASSIFICATION/DOWNGRADING SCHEDULE	
4. PERFORMING ORGANIZATION REPORT NUMBER(S) NRL Report 8796	5. MONITORING ORGANIZATION REPORT NUMBER(S)
6a. NAME OF PERFORMING ORGANIZATION Naval Research Laboratory 6b. OFFICE SYMBOL *(If applicable)*	7a. NAME OF MONITORING ORGANIZATION
6c. ADDRESS *(City, State and ZIP Code)* Washington, DC 20375	7b. ADDRESS *(City, State and ZIP Code)*
8a. NAME OF FUNDING/SPONSORING ORGANIZATION Office of Naval Research 8b. OFFICE SYMBOL *(If applicable)*	9. PROCUREMENT INSTRUMENT IDENTIFICATION NUMBER
8c. ADDRESS *(City, State and ZIP Code)* Arlington, VA 22217	10. SOURCE OF FUNDING NOS. PROGRAM ELEMENT NO.: 61153N; PROJECT NO.: 021-05-43; TASK NO.: 53; WORK UNIT NO.: 0626-00
11. TITLE *(Include Security Classification)* (See Title on Page ii)	
12. PERSONAL AUTHOR(S) Ben H. Cantrell	
13a. TYPE OF REPORT Interim 13b. TIME COVERED FROM _____ TO _____	14. DATE OF REPORT *(Yr., Mo., Day)* 1984 April 6 15. PAGE COUNT 32
16. SUPPLEMENTARY NOTATION	
17. COSATI CODES FIELD / GROUP / SUB. GR.	18. SUBJECT TERMS *(Continue on reverse if necessary and identify by block number)* Detection, Radar signal processing, Video integration, Target detection

19. ABSTRACT *(Continue on reverse if necessary and identify by block number)*

Six integrators used in long-term radar integration were studied. Generally, we found, even in fairly dense background of targets, that there was significant improvement in target detection due to the long-term integration and that the false-target generation could be controlled. The mechanism that allowed this result is based on removing a small percentage of the strongest signal in each integrator. This mechanism removed the few true target signals in many of the integrators which could cause *ghost* detections that were not valid targets. Using this technique, the false detections were easily controlled at only a very small expense in true target detectability.

20. DISTRIBUTION/AVAILABILITY OF ABSTRACT UNCLASSIFIED/UNLIMITED ☐ SAME AS RPT. ☐ DTIC USERS ☐	21. ABSTRACT SECURITY CLASSIFICATION
22a. NAME OF RESPONSIBLE INDIVIDUAL	22b. TELEPHONE NUMBER *(Include Area Code)* 22c. OFFICE SYMBOL

DD FORM 1473, 83 APR EDITION OF 1 JAN 73 IS OBSOLETE.

SECURITY CLASSIFICATION OF THIS PAGE

11. TITLE (Include Security Classification) (Continued)

COMPARISON OF SIX INTEGRATORS USED IN LONG-TERM RADAR INTEGRATIONS

CONTENTS

INTRODUCTION 1

DEFINITIONS 1

Amplitude Samples and Linear Motion 1
Integration Equations 3
Models for Noise and Signals 3

PROBABILITY OF FALSE DETECTION (False Alarm) 4

Ordinary Simulation Procedure 4
Importance Sampling 5
Noise-Only Results 6
False Detections Including *Ghost* Conditions 8

PROBABILITY OF DETECTION 8

Procedure 8
Detection Results 13

COMPARISON OF INTEGRATORS 20

S/N Improvement 20
False Detection Control 26
Discussion 28

SUMMARY 28

REFERENCES 29

COMPARISON OF SIX INTEGRATORS USED IN LONG-TERM RADAR INTEGRATIONS

INTRODUCTION

Because radar signals from targets persist over time, detection improvement can be obtained against noise, clutter, and interference which have different characteristics through signal processing such as integration. Most of the integration studies, coherent or noncoherent, have been conducted on target signals which do not move appreciably in range or azimuth during the processing time [1]. However, some work has been conducted on integration over long time frames where target motion is appreciable [2, 3]. In these studied, binary integration was studied using integrations which accounted for linear target motion. Basically an intermediate threshold was set which allowed a considerable number of detections. Then the final detector required at least a given number of detections to be present for any possible target motion. From these studies, it appears that both detection and false-alarm control improvement can be obtained.

We compare the characteristics of six different long-term integrators which account for linear target motion. In particular, we are concerned with dense target environments. Can we properly sort out the true targets in the dense set of signals, (or control the false detections), and still obtain a significant improvement in target detectability due to long-term integration? This situation can arise in sensitive radars which will detect insects, birds, angels, etc., as well as air targets of interest, some of which may be about the same size. A very similar situation arises when there are targets embedded in spikey clutter. After all the targets are obtained, the ones of interest can be chosen on the basis of velocity.

We begin the study by defining the six integrators, and the models for the signals and noise. Only range motion is considered for simplicity. It is impossible to study every possible situation, but the models investigated are representative. We determine the thresholds required to maintain fixed probabilities of false alarms for a number of background target conditions, length of integration, etc. We then determine the probability of detection for the same conditions. Finally, a discussion of the results is given.

DEFINITIONS

Amplitude Samples and Linear Motion

We define complex amplitude samples of the baseband radar signal as

$$X(n,\ k),$$

where $n = 0, \text{---} (N_s - 1)$ dwells and $k = 1, \text{---} K_0$ range cells. The N_s radar dwells and K_0 range cells are collected at uniform spacings in time and space. The magnitude of $X(n,\ k)$ is designated $|X(n,\ k)|$.

An index k' describing linear range motion is

$$k' = k - I\left[\frac{np}{N_s - 1}\right],$$

Manuscript approved November 7, 1983.

where p is an integer index which represents the p-th range velocity which takes on values from $-P_0$ to P_0. The symbol I means round the quotient to the nearest integer. Beginning with the range cell k on the $n = 0$ dwell, the target exhibiting linear motion with velocity p will be located at the k' range cell on the nth dwell. The spacings between adjacent velocity indices is set such that there is one range cell change over N_s dwells between indexes of p and $p + 1$. The value of P_0 is set by

$$P_0 = I\left\{\frac{\text{maximum radial distance a target moves in } N_s \text{ dwells}}{\text{range resolution of radar}}\right\}.$$

Although not necessary, the notation in the subsequent development becomes much simpler if we rank order the amplitudes of the samples used in each integrator. For each value of k' formed from a range k and velocity p, the $n = 0$ through $N_s - 1$ samples of $|X\ (n,\ k')|$ are rank ordered in amplitude and defined by

$\lvert X_r\ (0,\ k,\ p)\rvert$	smallest values of $\lvert X\ (n,\ k')\rvert$ for $n = D,$ --- $(N_s - 1)$ given k and p
$\lvert X_r\ (1,\ k,\ p)\rvert$	next smallest value of $\lvert X\ (n,\ k')\rvert$ for $n = 0,$ --- $(N_s - 1)$ given k and p
—	—
—	—
—	—
—	—
$\lvert X_r\ ((N_s - 1),\ k,\ p)\rvert$	largest value of $\lvert X\ (n,\ k')\rvert$ for $n = 0,$ --- $(N_s - 1)$ given k and p.

This operation is performed for each new integration defined by p and k.

Figure 1 illustrates radar amplitude $|X\ (n,\ k)|$ samples of a fast and slow linear motion target when there is no noise present. The object of the integration is to use the target signals over all dwells N_s in the detection process despite its motion in range. Since the target location and speed is unknown, all possible candidates must be observed.

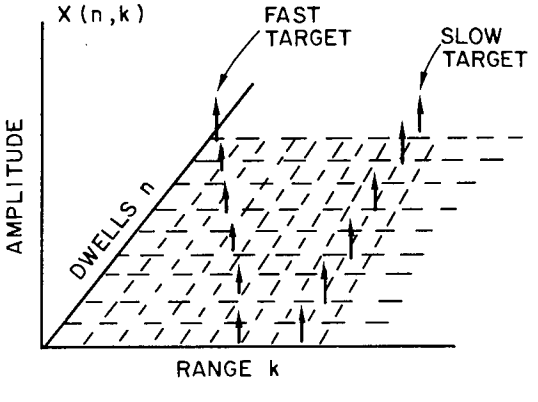

Fig. 1 — Representation of noise-free signals before integration

Integration Equations

Two variants of three standard radar video integrators are compared; (1) square law, (2) linear, (3) optimum (M out of N_s) binary, (4) square law minus largest sample, (5) linear minus largest sample, and (6) $M + 1$ out of N_s binary integrators. These equations are:

Square Law

$$Y_1(p,k) = \sum_{n=0}^{N_s-1} |X_r\ (n,\ k,\ p)|^2$$

Linear

$$Y_2(p,k) = \sum_{n=0}^{N_s-1} |X_r\ (n,\ k,\ p)|$$

Binary (M out of N_s)

$$Y_3(p,k) = |X_r\ (N_s - M,\ k,\ p)|$$

Square Law Minus Largest Sample

$$Y_4(p,k) = \sum_{n=0}^{N_s-2} |X_r\ (n,\ k,\ p)|^2$$

Linear Minus Largest Sample

$$Y_5(p,k) = \sum_{n=0}^{N_s-2} |X_r\ (n,\ k,\ p)|$$

Binary ($M + 1$) out of N_s

$$Y_6(p,k) = |X_r\ (N_s - M - 1,\ k,\ p)|.$$

When a target is traversing with linear motion there will be one integrator output which will contain target signals in all N_s dwells of the samples used in the integration. Figure 2 illustrates the integrator output magnitude at the matched filter index location of range k and velocity p for two different targets. The contributions due to these targets in other filters are not shown. As in other radar integrators, an improvement in detection performance is expected. However, because of the linear motion of the indexes, some target signals can appear in other than the intended integrator's outputs. The last three integrators, as discussed more thoroughly later, are designed to minimize this effect of a signal entering an integrator which does not contain a valid target.

Models for Noise and Signals

Conventional radar signals can be expressed as

$$X(n,k) = S_N(n,k) + S_T(n,k),$$

where $S_N(n,k)$ is a complex number representing noise, and $S_T(n,k)$ is a complex number representing signal. The usual radar thermal noise is expressed

$$S_N(n,k) = g_I + j\ g_Q,$$

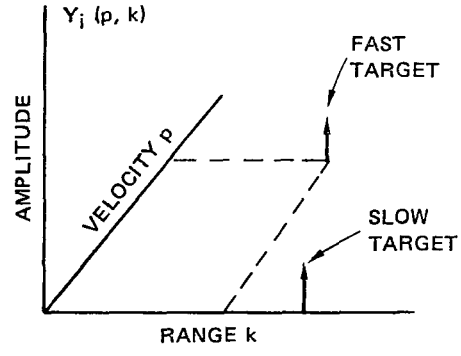

Fig. 2 — Representation of noise-free signals after integration

where g_I and g_Q are independent zero mean Gaussian distributed random variables with standard deviation $\tilde{\sigma}_T$ and j is the square root of minus one. New samples are taken for each value of n and k and each new trial.

For the signal $S_T(n,k)$, we generate N_t Rayleigh fluctuating targets randomly distributed in range and velocity exhibiting linear motion. Furthermore, each target is assigned a random signal-to-noise ratio (S/N). This can be accomplished in two stages by first obtaining intermediate signals

$$S_a(i,\ n,\ k) = \begin{cases} g_I + jg_Q \text{ for } k = k^*(i) - I\left[\dfrac{np^*(i)}{N_s - 1}\right] \\ 0 \qquad \text{for all other } k, \end{cases}$$

where g_I, and g_Q are independent zero mean Gaussian distributed random variables with standard deviation $\hat{\sigma}_T(i)$, $k^*(i)$ and $p^*(i)$ are the location of the ith target in range and velocity, respectively, and $S_a(i,\ n,\ k)$ is the intermediate signal of the ith target. The total signal is given by

$$S_T(n,k) = \sum_{i=1}^{N_t} S_a(i,\ n,\ k).$$

The reason a two-step process was necessary was that more than one target was allowed to occupy the same range and dwell sample. The signal standard deviation is Rayleigh distributed with standard deviation of $\bar{\sigma}_T$. Consequently, the average signal-to-noise ratio $\overline{S/N}$ is given by $\bar{\sigma}_T/\tilde{\sigma}_T$. Finally, we define a target density ρ by

$$\rho = \frac{N_t}{K_0},$$

which has dimension of targets per range cell.

PROBABILITY OF FALSE DETECTION (False Alarm)

Ordinary Simulation Procedure

The probability of false detection is studied using Monte Carlo simulation. A computer is used to emulate the integrators which operate on computer generated signals of the type previously described. Using many trials, a histogram or probability density of the output signal $Y_i(p,k)$ amplitude is found. The output signal is broken into L equally spaced intervals of width d which spans all reasonably likely values of $Y_i(p,k)$. The lth interval is computed by

$$l = I\left[\frac{Y_i(p,k)}{d}\right],$$

where l can take on values from zero through L. We count the number of times the signal $Y_i(p,k)$ falls into each interval l over a number of trials and divide by the number of trials to obtain a rough estimate of the probability density. This procedure can be accomplished recursively for each new range and velocity by

$$f(l) = f(l) + \delta(p,k)/N_D,$$

where $\delta(p, k)$ is one for ordinary Monte Carlo simulation, N_D is the total number of trials, and $f(l)$ is the output probability density of the integrators. Initially we set $f(l) = 0$ for all l.

The probability of false detection, defined as the probability of $Y_i(p,k)$ exceeding a threshold l^* given no signal is present, can be obtained from

$$p_f = \sum_{l=l^*}^{L} f(l).$$

The normalized threshold is defined as

$$\gamma = dl^*/\tilde{\sigma}_T.$$

Consequently, we obtain the probability of false detection p_f as a function of the normalized threshold γ.

Two subsets of signals in $Y_i(p,k)$ are excluded from being used in forming the histogram and, consequently, not included in the probability of false detections. First, the edge effects are removed by excluding the first and last P_0 range cells in $Y_i(p,k)$. Second, any valid target will cause signal to be present in a number of neighboring range and velocity cells as well as the intended one. Under normal circumstances, target reports from these neighboring cells would be merged into the valid target report range and velocity cell. Consequently, we exclude all range and velocity cells which are likely to contain approximately two or more signals. Figure 3 shows this region of space for the given target.

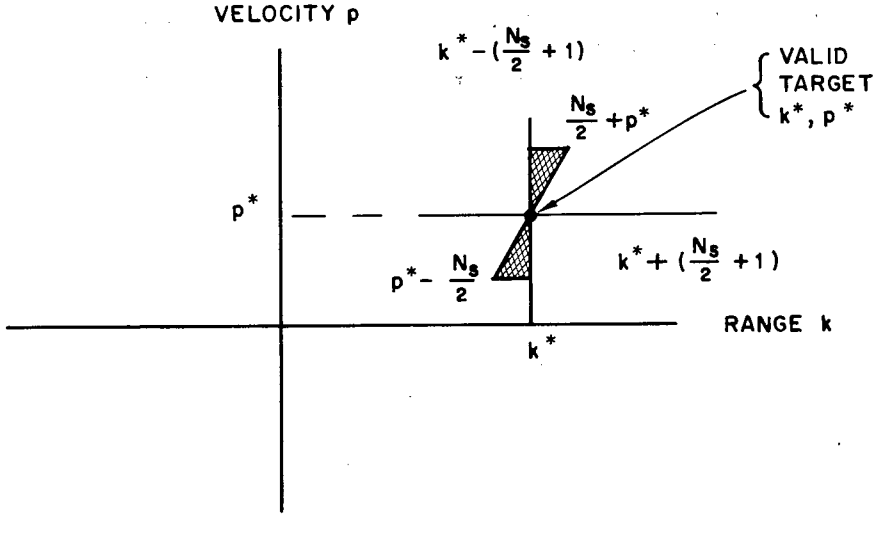

Fig. 3 — Signals in cross-hatched region not included in signals used for computing the probability of false detection

Importance Sampling

To circumvent using a very large number of samples when we wish to study low probability of occurrence events, a technique called importance sampling [4, 5] is used. The basic procedure is to distort the probability densities used in an ordinary Monte Carlo simulation such that more events of

interest occur than usual and then correct the measured statistics based on the distortion and samples. This technique reduces the number of required samples and works well as long as the mechanisms which cause the rare events are the same under no distortion and distortion.

The importance sampling is implemented as follows. We define the weight $\delta(p,k)$ used in the formation of the histogram as

$$\delta(p,k) = \prod_{n=0}^{N_s-1} W_N(n,k')\ W_S(n,k') \text{ where } k' = k - I\left[\frac{np}{N_s - 1}\right].$$

$W_N(n,k')$ is a weight which is evaluated by using only the noise portion of the sample $X(n,k')$, and $W_S(n,k')$ is a weight which is evaluated by using only the signal portion of the sample $X(n,k')$. If no signal is present, then $W_S(n,k')$ is one.

Specifically, we define $W_N(n,k')$ as the ratio of the true probability density to the distorted probability density evaluated at the noise sample values from the Gaussian-distributed random number generator. This is given by

$$W_N(n,k') = \frac{\tilde{\sigma}_D^2}{\tilde{\sigma}_T^2} \exp\left\{-\frac{1}{2}\left[\frac{\tilde{\sigma}_T^2 - \tilde{\sigma}_D^2}{\tilde{\sigma}_T^2\,\tilde{\sigma}_D^2}\right] |S_N(n,k')|^2\right\},$$

where $\tilde{\sigma}_D$ is the standard deviation of the distorted Gaussian distributed probability density.

Because more than one target is allowed to occupy the same range cell on the same dwell, the computation of the $W_S(n,k')$ is slightly more complicated. We first compute an intermediate weight $W_a(i,n,k'^*)$ based on the ith target by

$$W_a(i,n,k') = R\ \frac{\hat{\sigma}_D^2(i)}{\hat{\sigma}_T^2(i)} \exp\left\{-\frac{1}{2}\left[\frac{\hat{\sigma}_T^2(i) - \hat{\sigma}_D^2(i)}{\hat{\sigma}_T^2(i)\ \hat{\sigma}_D^2(i)}\right] |S_a(i,n,k')|^2\right\},$$

where $\hat{\sigma}_D(i)$ is the standard deviation of the distorted Gaussian distributed target signal of the ith target, and R is ratio of the true number of targets to the number of targets generated under distortion. The weight $W_a(i,n,k')$ is generated for only those values where $S_a(i,n,k')$ has a nonzero value. Then we find

$$W_S(n,k') = \prod_{i=1}^{N_t} W_a(i,n,k').$$

Noise-Only Results

We determined the probability of false detection when no targets were present. The high probability of false detections were obtained by using the ordinary Monte Carlo simulations, and the small probability of false detections were obtained by using the importance sampling technique. In these cases $W_S(n,k')$ was always equal to one. Figures 4 to 9 show the results of the six integrators for $P_0 = 4\ N_s$. The results in Figs. 4 to 6 also can be found in Refs. 6 to 8. The value of M that was used in the binary integrator is the optimum one found in Ref. 8 for ordinary noncoherent integration. The thresholds in Figs. 7 to 9 for a given probability of a false detection are a little less than those in Figs. 4 to 6 because of the removal of the largest sample or requirement of one more intermediate detection. Even though the probability of false detection at any given range and velocity vs normalized threshold is the same as standard noncoherent integration found in the literature, the overall number of false detections on a radar is higher because of the $(2P_0 + 1)$ times more opportunities. However, the false detections are correlated over a finite period of time.

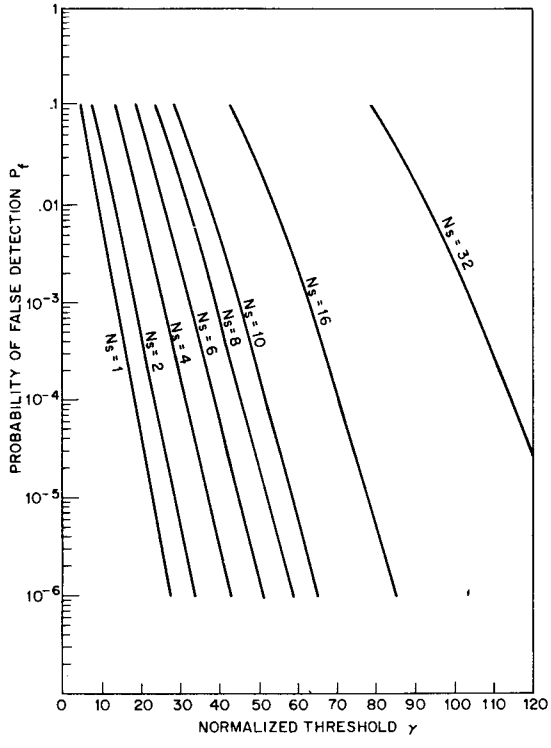

Fig. 4 — Probability of false detection vs normalized threshold given noise background (square law integrator)

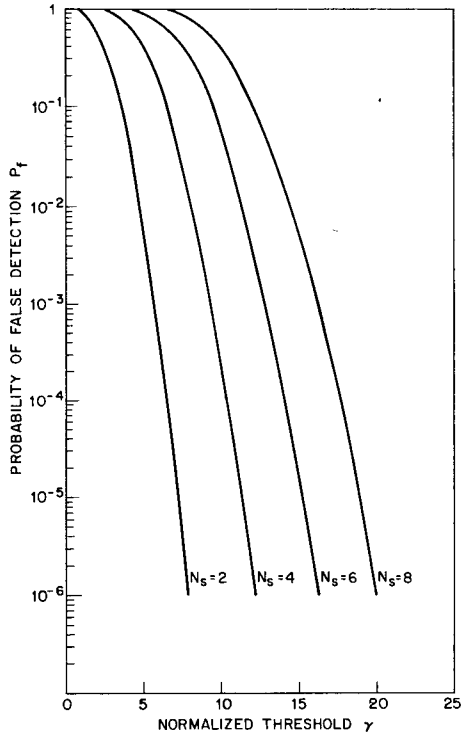

Fig. 5 — Probability of false detection vs normalized threshold given noise background (linear integrator)

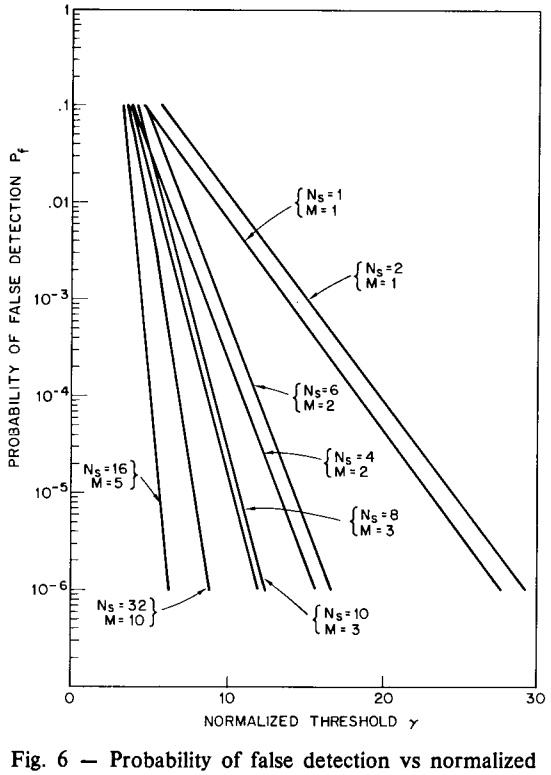

Fig. 6 — Probability of false detection vs normalized threshold given noise background (binary integrator)

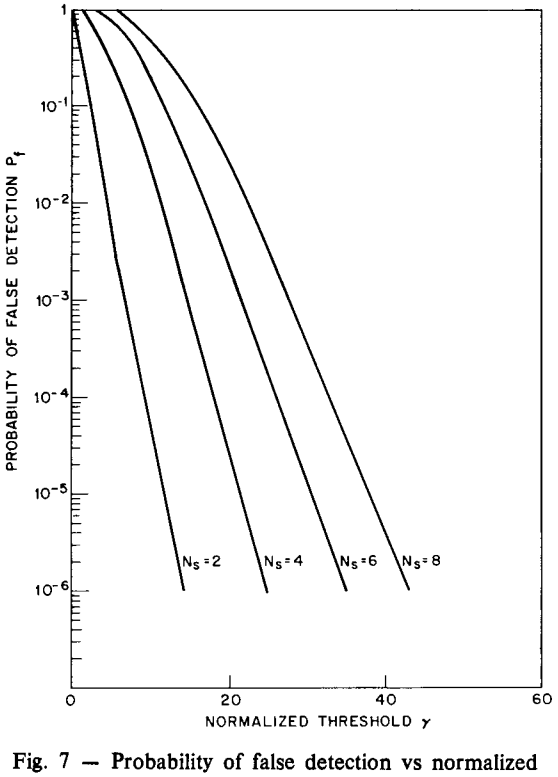

Fig. 7 — Probability of false detection vs normalized threshold given noise background (square law-largest integrator)

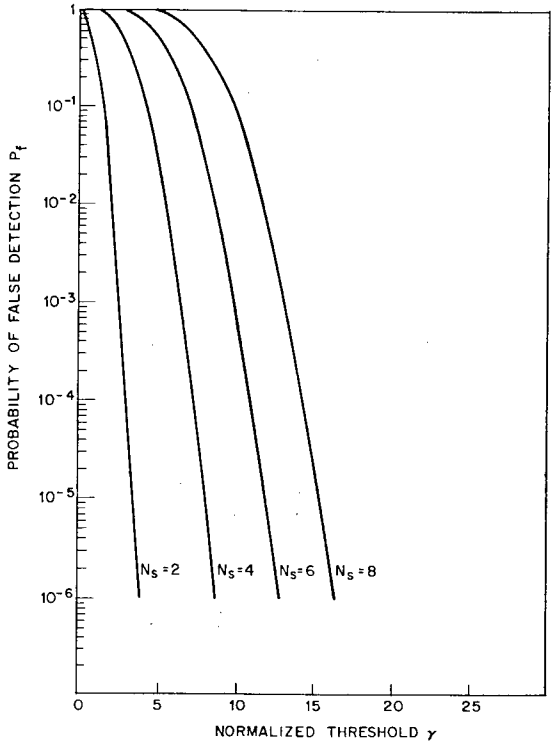

Fig. 8 — Probability of false detection vs normalized threshold given noise background (linear-largest integrator)

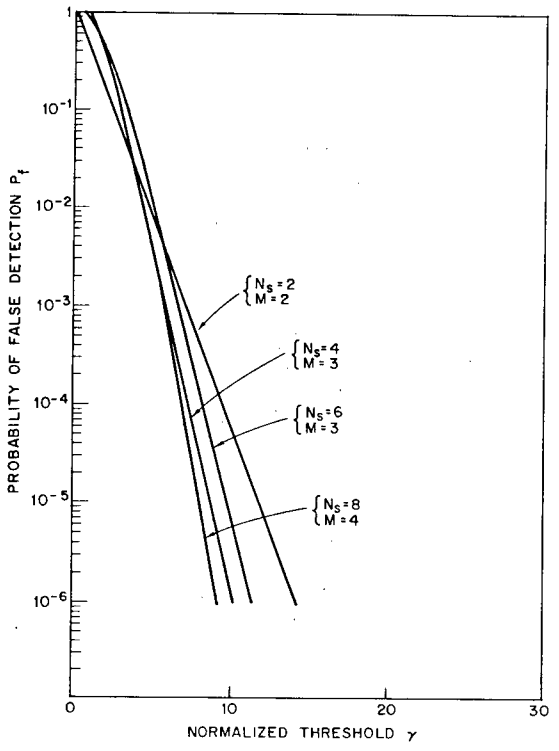

Fig. 9 — Probability of false detection vs normalized threshold given noise background ($M + 1$ binary integrator)

False Detections Including *Ghost* Conditions

We next introduce target signals which can produce *ghost* detections due to target signals at ranges and velocities that contain no real target. This can occur because an integrator can pick up a signal from another target due to range index changes caused by the linear motion. Again we set $P_0 = 4\ N_s$. The probability of a false detection vs normalized threshold for the six integrators is shown in Figs. 10 to 15 for a target density of $\rho = 0.1$ and an $\overline{S/N} = 10$ dB, in Figs. 16 to 21 for a target density of $\rho = 0.01$ and a $\overline{S/N} = 10$ dB, and in Figs. 22 to 27 for a target density of $\rho = 0.1$ and an $\overline{S/N} = 3$ dB.

Observing these figures, we find generally that (a) the threshold must be raised when signals are present to maintain the same false alarm rate as noise only; (b) the higher the signal amplitude, the more the thresholds must be raised, (c) the higher the target density, the higher the thresholds must be raised to maintain constant false detection rates; and (d) the integrators which remove the largest sample or require higher values of M in the binary integrator do not require nearly as high thresholds to maintain the same false detection rates. These generated thresholds are used subsequently in determining the probability of detection.

PROBABILITY OF DETECTION

Procedure

The probability of detection was obtained in the same manner as the probability of false detection described previously, except only those range and velocity cells in the integrator output which are matched to the target and contain signals are used in generating the statistics. To save computation, we generated the signal and noise for each integrator by using one target only and ignored the case in which two or more targets occupy the same range on the same dwell. The only effect this has on the results is to produce a small, pessimistic error in the estimate of the probability of detection.

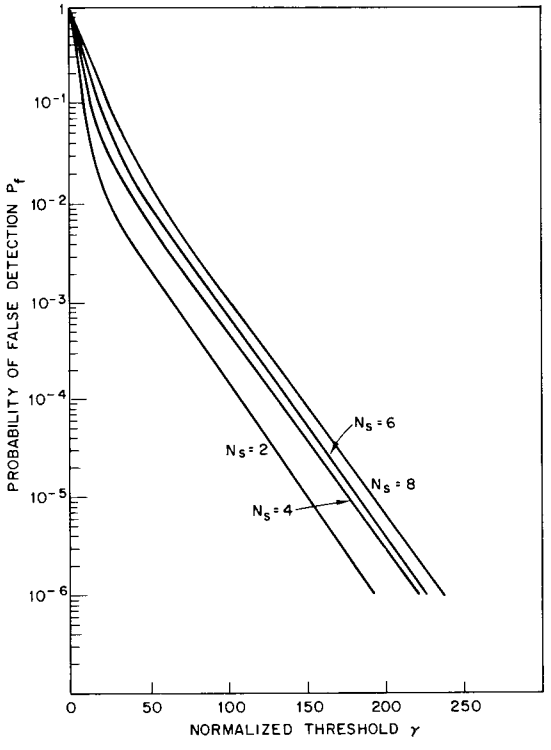

Fig. 10 — Probability of false detection vs normalized threshold for $\rho = 0.1$ and $(\overline{S/N}) = 10$ dB (square law integrator)

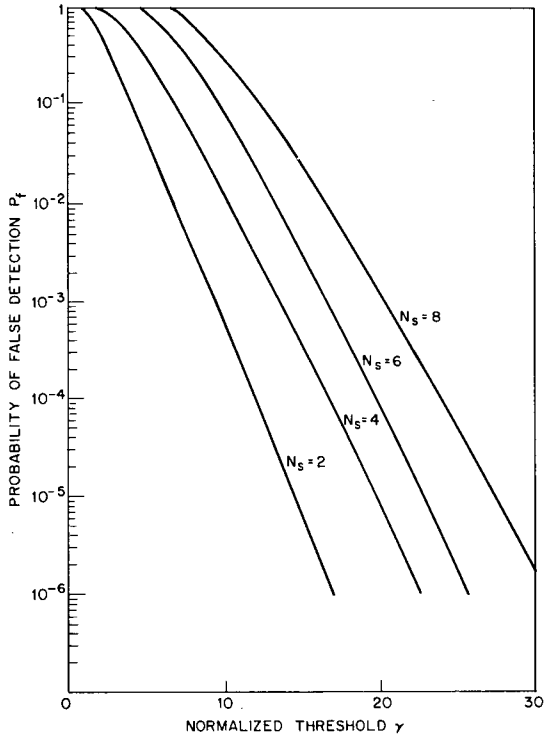

Fig. 11 — Probability of false detection vs normalized threshold for $\rho = 0.1$ and $(\overline{S/N}) = 10$ dB (linear integrator)

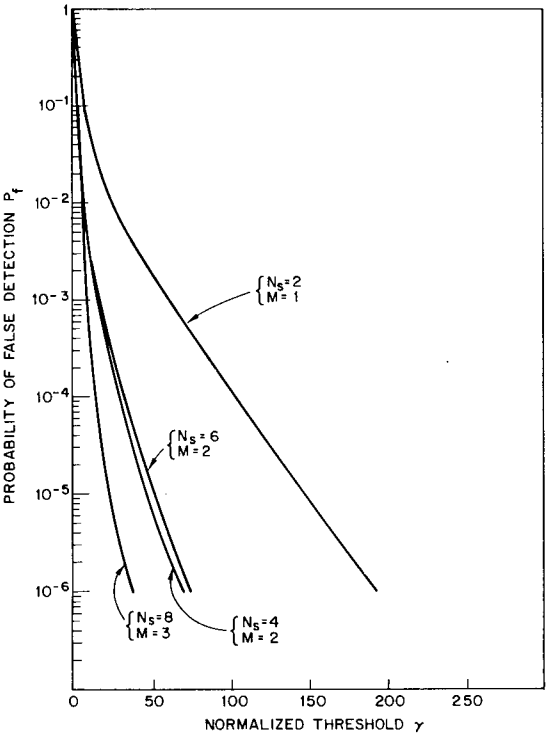

Fig. 12 — Probability of false detection vs normalized threshold for $\rho = 0.1$ and $(\overline{S/N}) = 10$ dB (binary integrator)

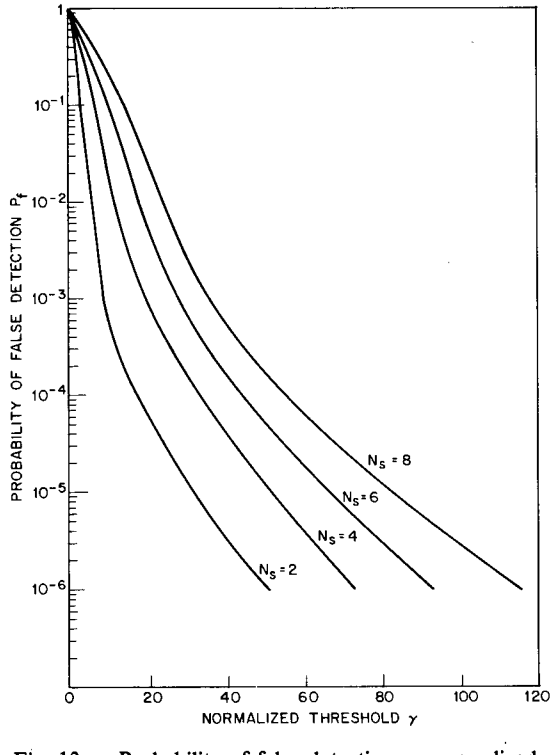

Fig. 13 — Probability of false detection vs normalized threshold $\rho = 0.1$ and $(\overline{S/N}) = 10$ dB (square law minus largest integrator)

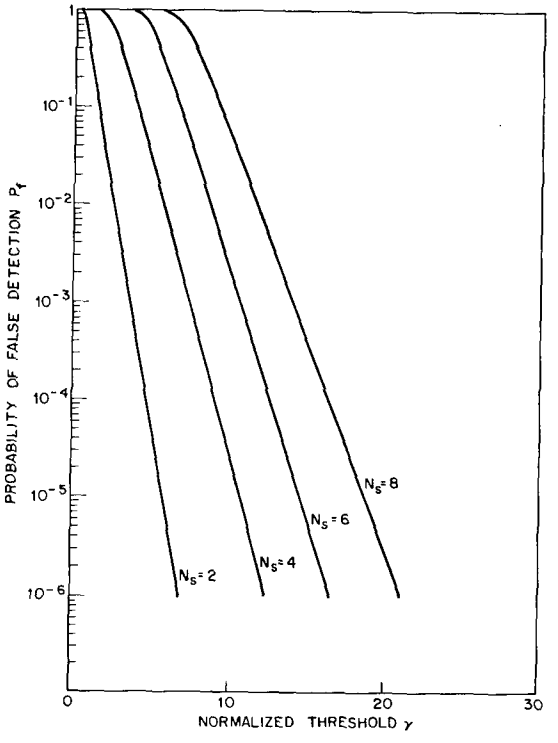

Fig. 14 — Probability of false detection vs normalized threshold for $\rho = 0.1$ and $(\overline{S/N}) = 10$ dB (linear minus largest integrator)

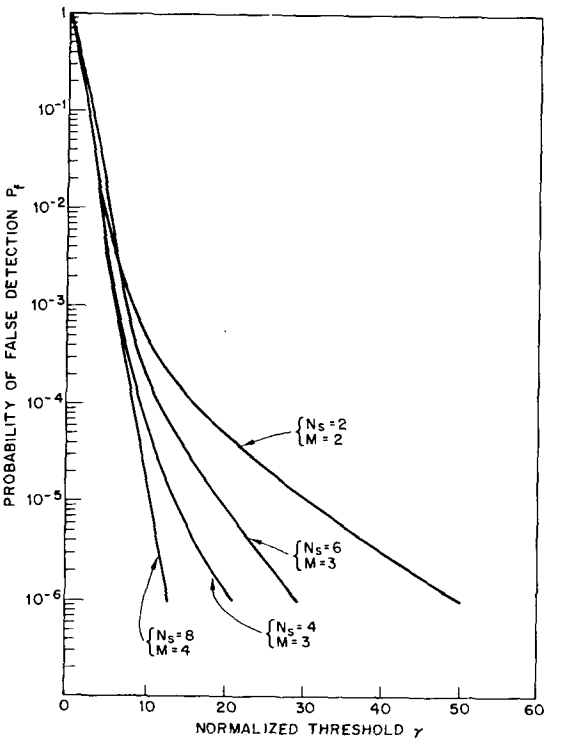

Fig. 15 — Probability of false detection vs normalized threshold for $\rho = 0.1$ and $(\overline{S/N}) = 10$ dB ($M + 1$ binary integrator)

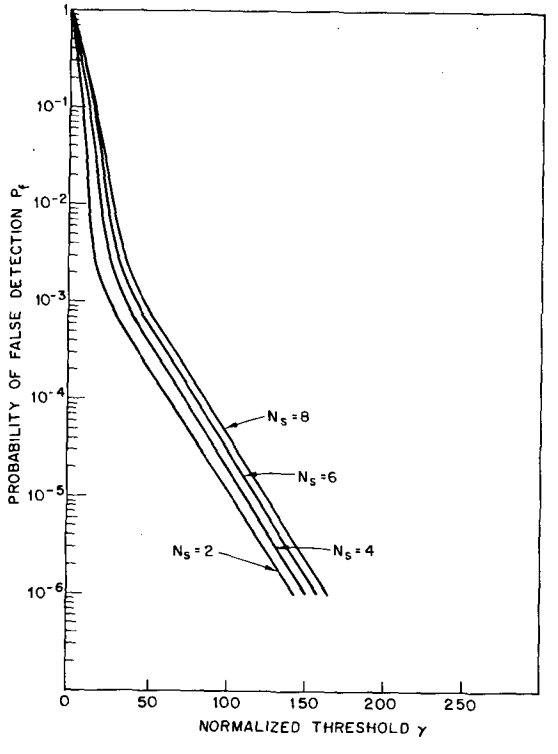

Fig. 16 — Probability of false detection vs normalized threshold for $\rho = 0.01$ and $(\overline{S/N}) = 10$ dB (square law integrator)

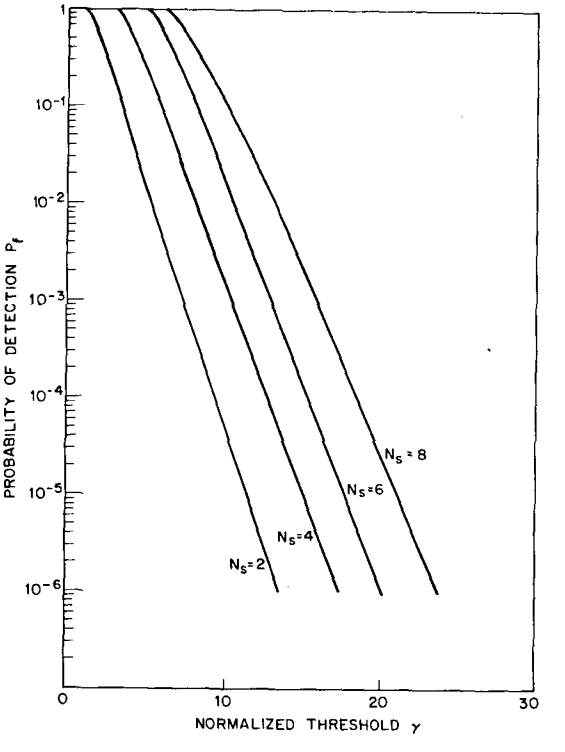

Fig. 17 — Probability of false detection vs normalized threshold for $\rho = 0.01$ and $(\overline{S/N}) = 10$ dB (linear integrator)

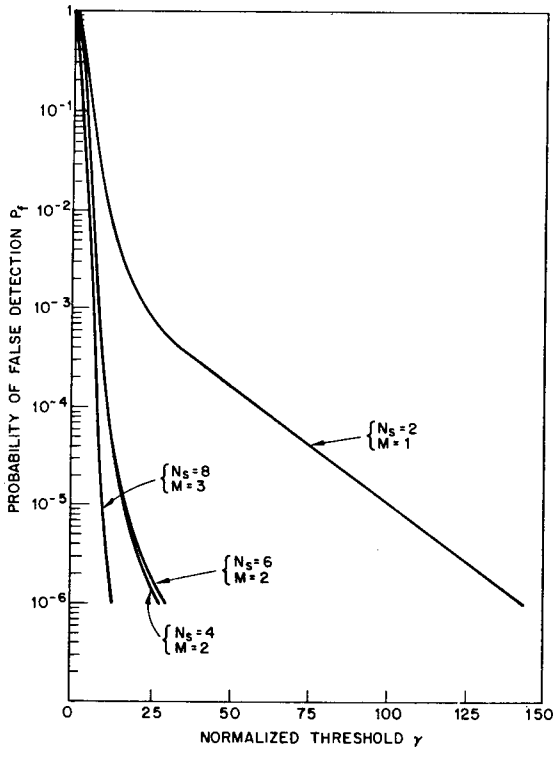

Fig. 18 — Probability of false detection vs normalized threshold for $\rho = 0.01$ and $(\overline{S/N}) = 10$ dB (binary integrator)

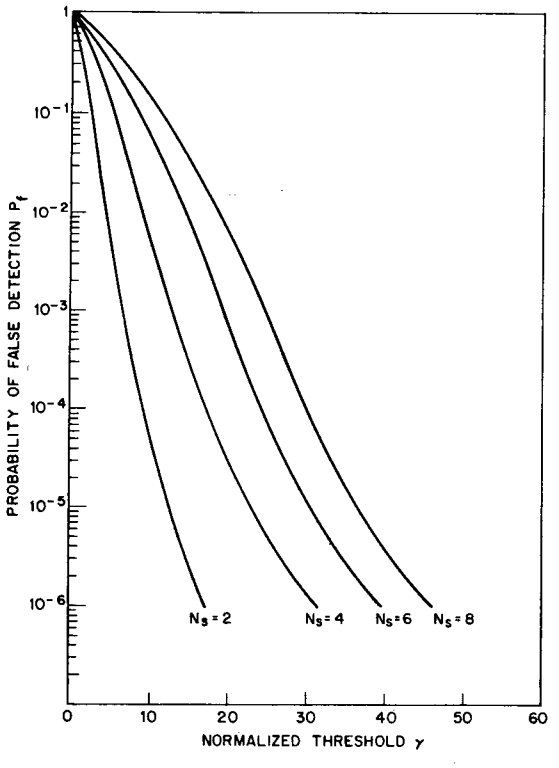

Fig. 19 — Probability of false detection vs normalized threshold for $\rho = 0.01$ and $(\overline{S/N}) = 10$ dB (square law-minus largest integrator)

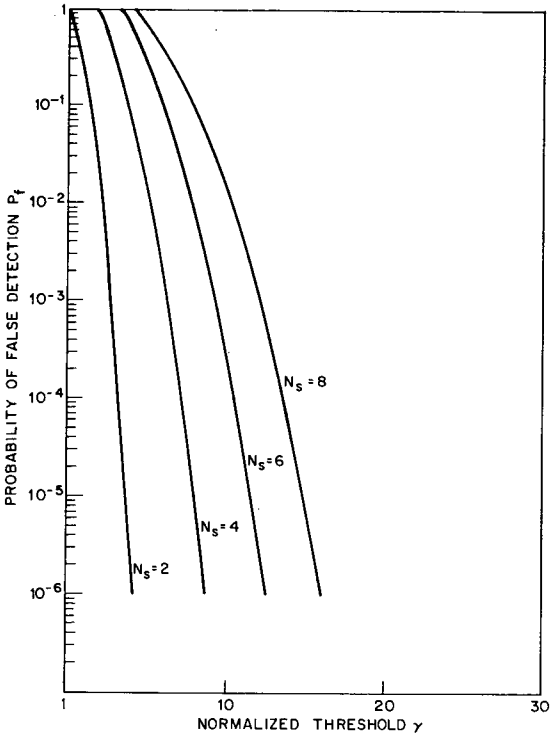

Fig. 20 — Probability of false detection vs normalized threshold for $\rho = 0.01$ and $(\overline{S/N}) = 10$ dB (linear-largest integrator)

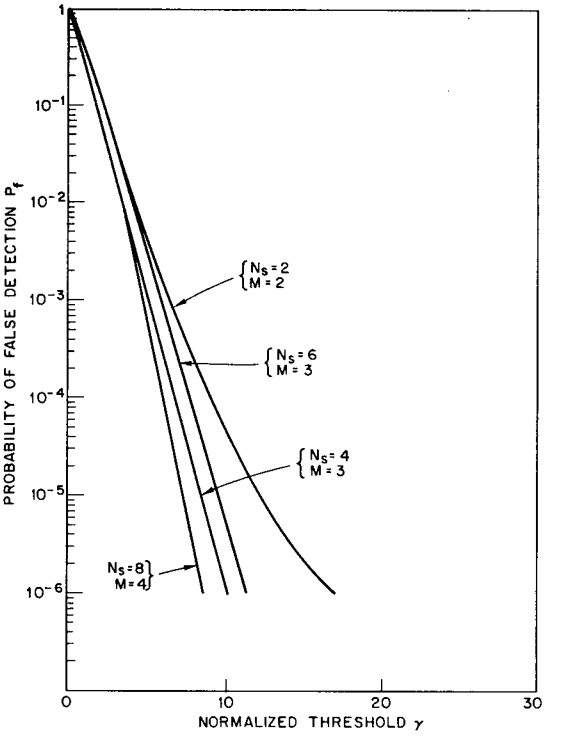

Fig. 21 — Probability of false detection vs normalized threshold for $\rho = 0.01$ and $(\overline{S/N}) = 10$ dB $(M + 1$ binary integrator)

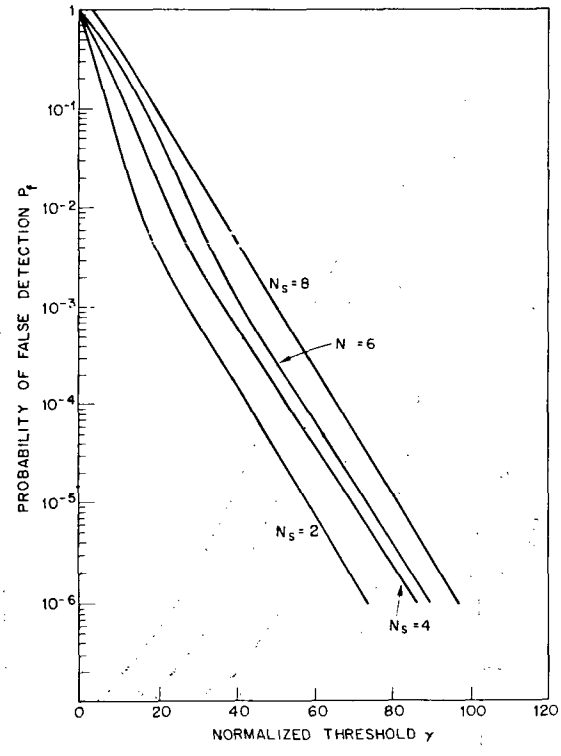

Fig. 22 — Probability of false detection vs normalized threshold for $\rho = 0.1$ and $(\overline{S/N}) = 3$ dB (square law integrator)

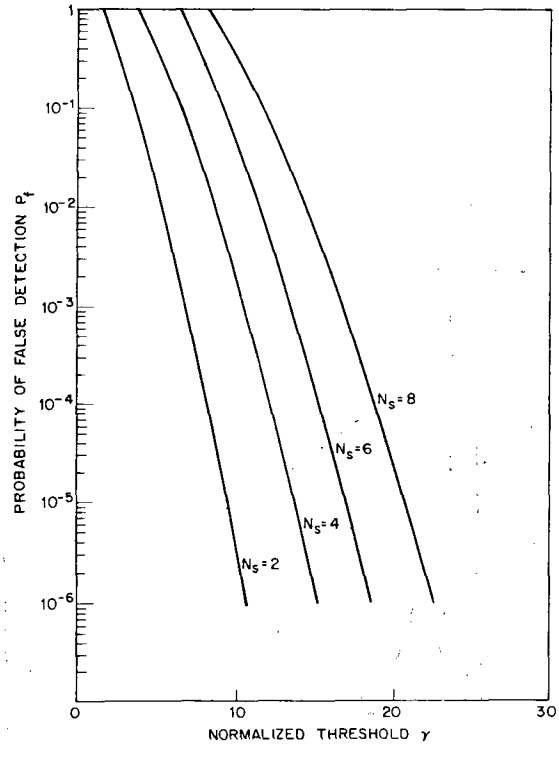

Fig. 23 — Probability of false detection vs normalized threshold for $\rho = 0.1$ and $(\overline{S/N}) = 3$ dB (linear integrator)

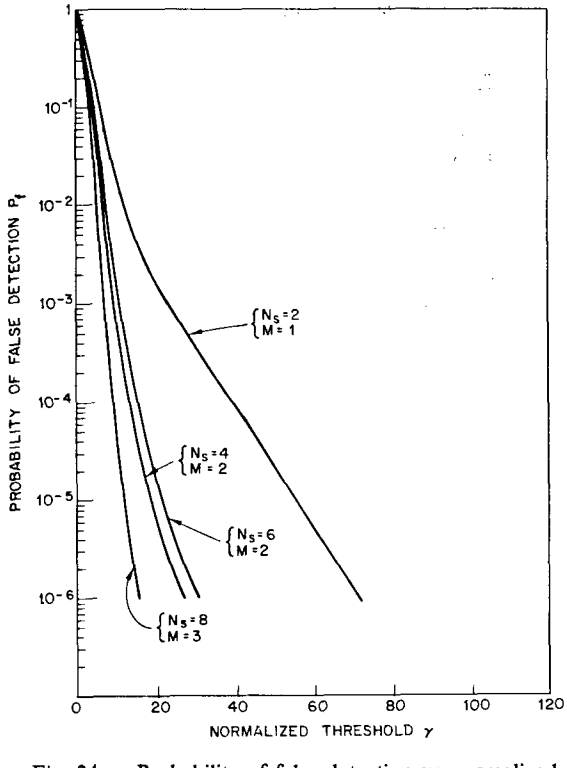

Fig. 24 — Probability of false detection vs normalized threshold for $\rho = 0.1$ and $(\overline{S/N}) = 3$ dB (binary integrator)

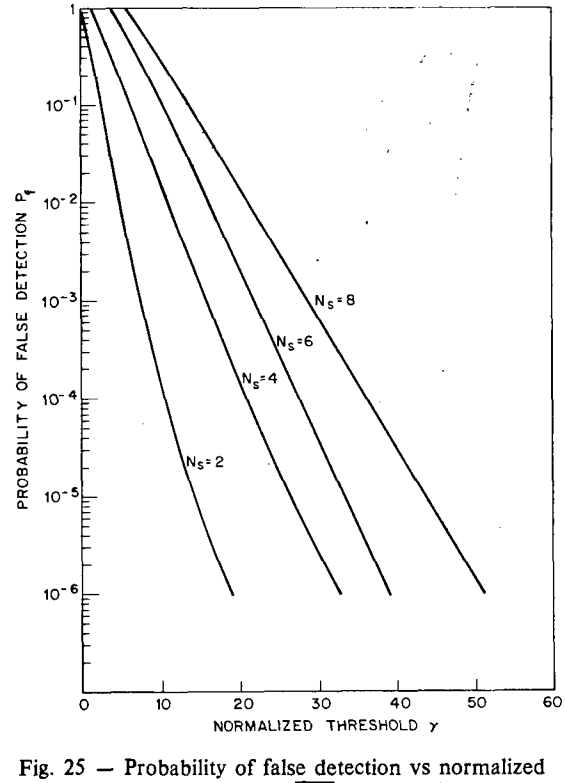

Fig. 25 — Probability of false detection vs normalized threshold for $\rho = 0.1$ and $(\overline{S/N}) = 3$ dB (square law minus largest integrator)

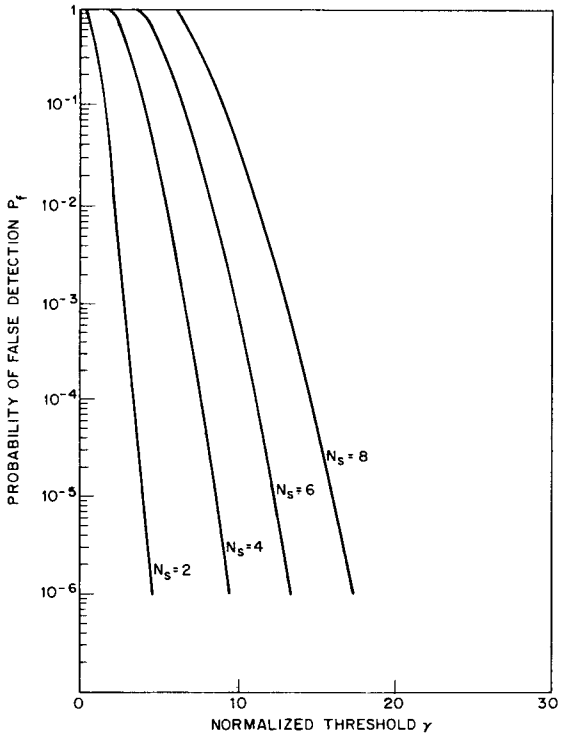

Fig. 26 — Probability of false detection vs normalized threshold for $\rho = 0.1$ and $(\overline{S/N}) = 3$ dB (linear minus largest integrator)

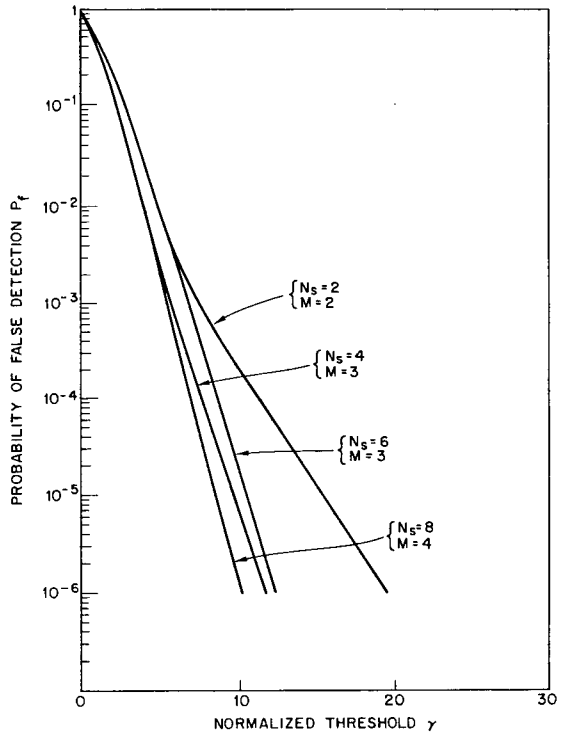

Fig. 27 — Probability of false detection vs normalized threshold for $\rho = 0.1$ and $(\overline{S/N}) = 3$ dB $(M + 1$ binary integrator)

Detection Results

All the probability of detections P_d are plotted vs (S/N) for a probability of false alarm of 10^{-6}. The thresholds required in the simulation are obtained from the probability of false detection vs normalized threshold curves previously generated and shown in Figs. 4 to 27. In all cases $P_0 = 4\ N_s$.

The probability of detection versus S/N for the six integrators are shown in Figs. 28 to 33 for the case of one target present. We find that the detection curves in Figs. 28 to 30 are the same as the standard detection curves for equivalent noncoherent integrators using Rayleigh fluctuating targets found in Ref. 1 Chapter 15, and Ref. 8. Figures 31 to 33 show small detection losses over those in Figs. 28 to 30 due to the removal of the largest sample or requiring $M + 1$ samples.

The probability of detection versus signal-to-noise ratio curves for $P_f = 10^{-6}$ for the six integrators are shown in Figs. 34 to 39. These curves were obtained by using higher thresholds caused by assuming a target density of $\rho = 0.1$ and an $\overline{S/N} = 10$ dB. In Figs. 40 to 45 detection curves are shown for a target density of $\rho = 0.01$ and a $\overline{S/N} = 10$ dB, and in Figs. 46 to 51 for a target density $\rho = 0.1$ and a $\overline{S/N} = 3$ dB.

Observing these figures, we find generally that (a) more detection losses occur for a higher background of other targets; (b) the larger the background targets amplitudes are, the more loss there is in detections; and (c) the integrators which remove the largest signals or require $M + 1$ detections suffer less detection loss than the other integrators when a background of other targets are present.

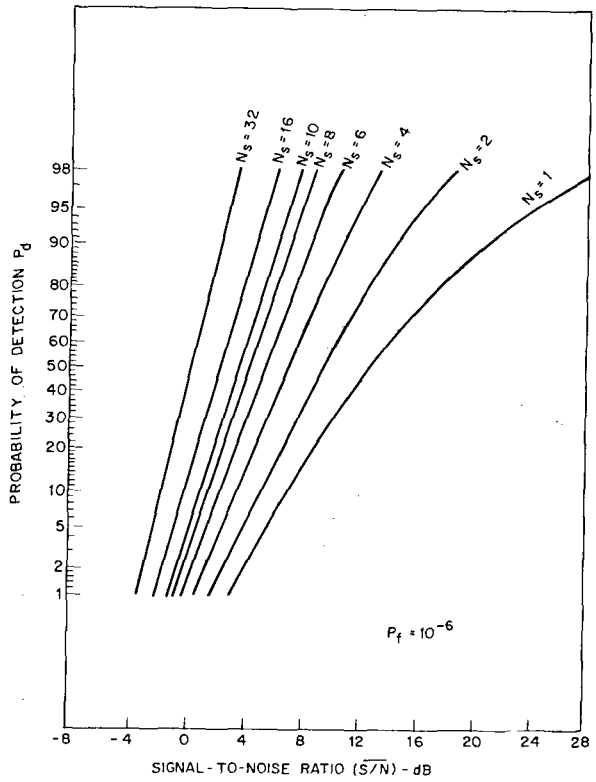

Fig. 28 — Probability of detection vs S/N given noise background (square law integrator)

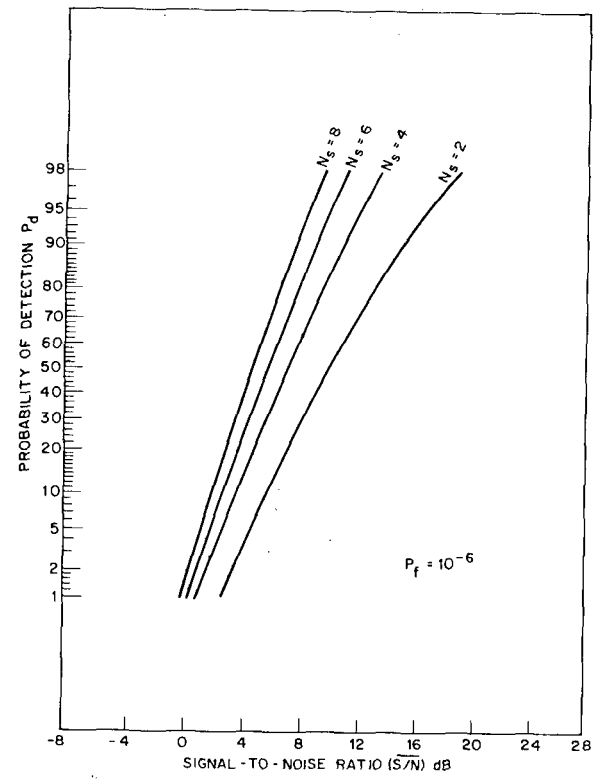

Fig. 29 — Probability of detection vs S/N given noise background (linear integrator)

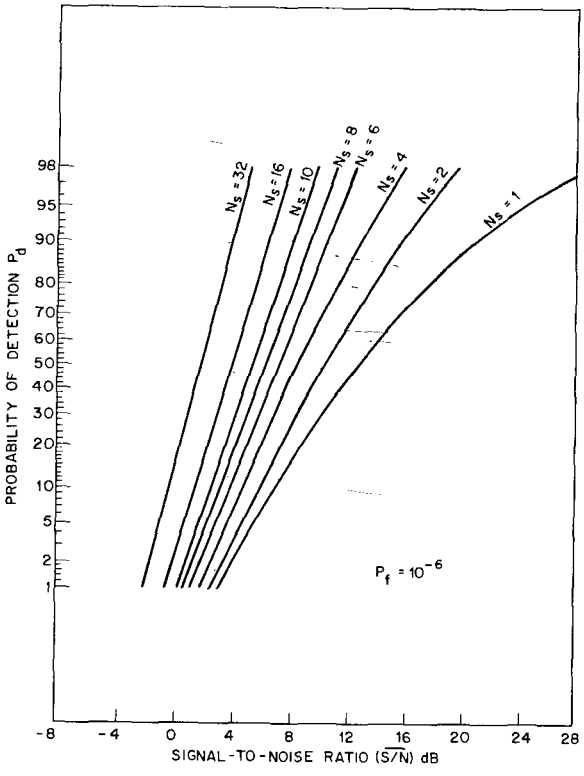

Fig. 30 — Probability of detection vs S/N given noise background (binary integrator)

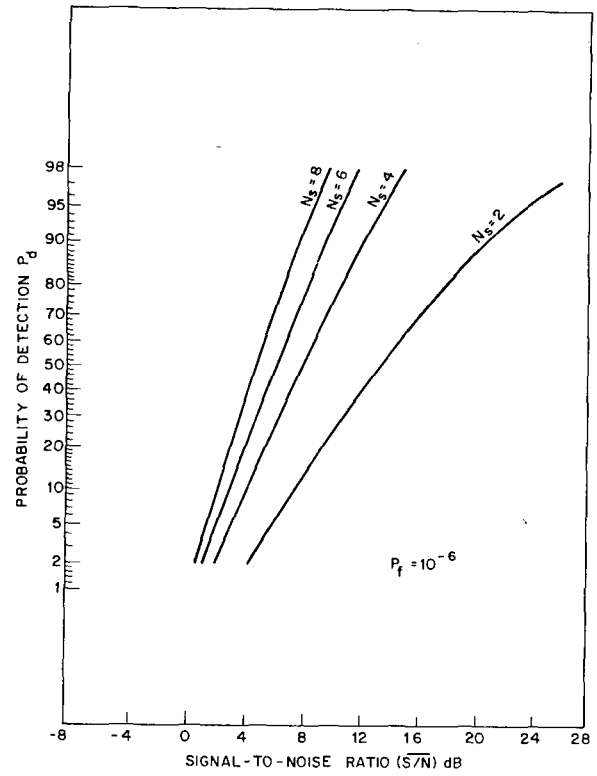

Fig. 31 — Probability of detection vs S/N given noise background (square law-largest integrator)

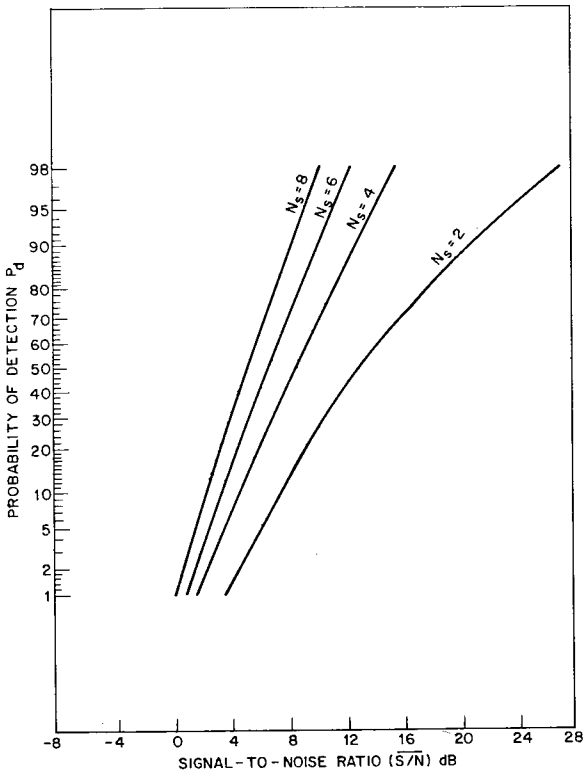

Fig. 32 — Probability of detection vs S/N given noise background (linear-largest integrator)

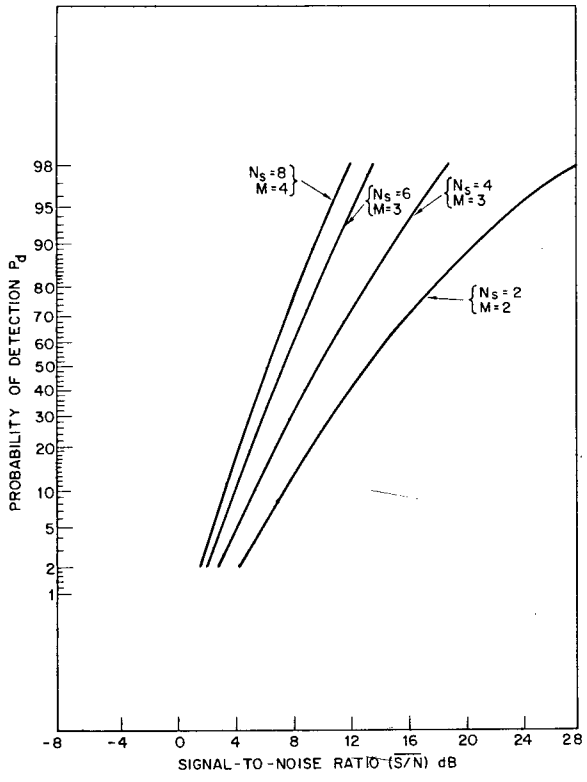

Fig. 33 — Probability of detection vs S/N given noise background ($M + 1$ binary integrator)

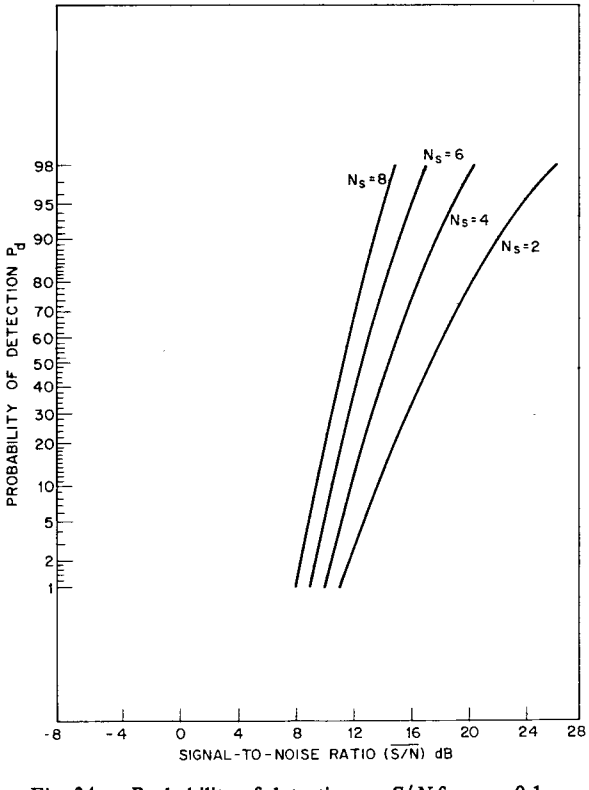

Fig. 34 — Probability of detection vs S/N for $\rho = 0.1$ and $(\overline{S/N}) = 10$ dB (square law integrator)

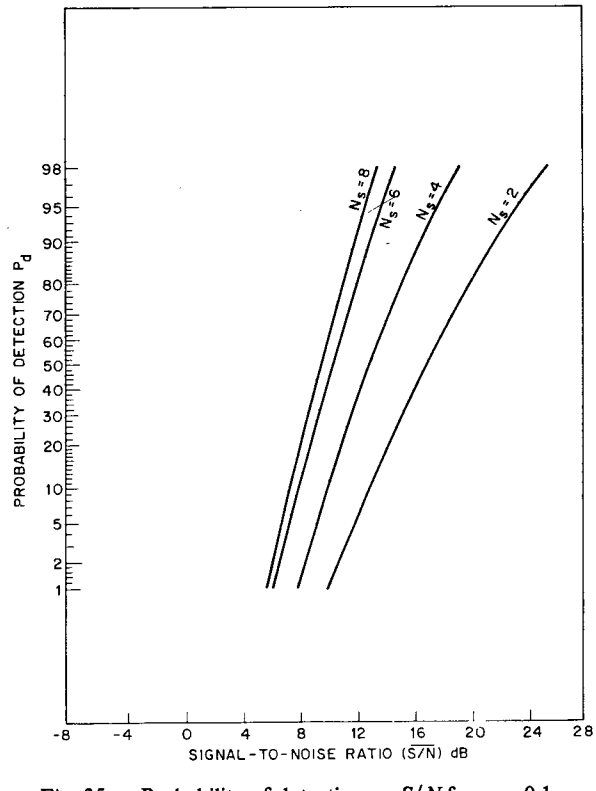

Fig. 35 — Probability of detection vs S/N for $\rho = 0.1$ and $(\overline{S/N}) = 10$ dB (linear integrator)

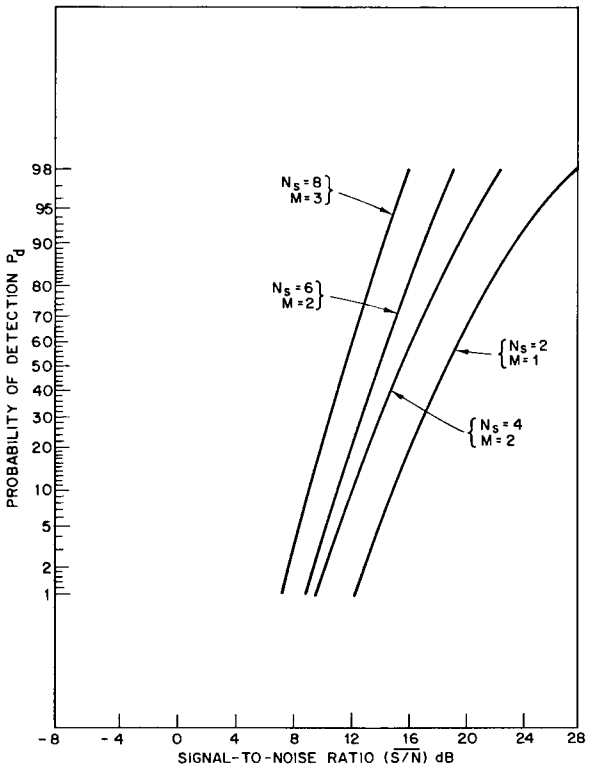

Fig. 36 — Probability of detection vs S/N for $\rho = 0.1$ and $(\overline{S/N}) = 10$ dB (binary integrator)

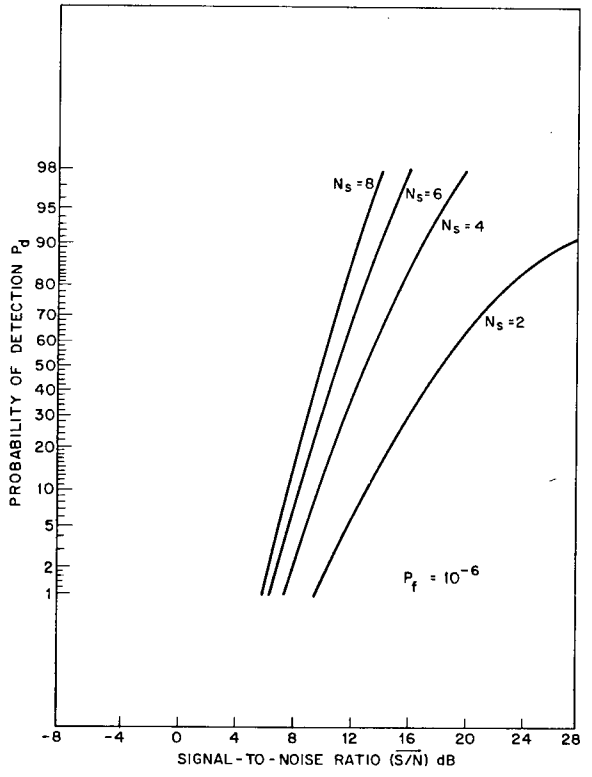

Fig. 37 — Probability of detection vs S/N for $\rho = 0.1$ and $(\overline{S/N}) = 10$ dB (square law minus largest integrator)

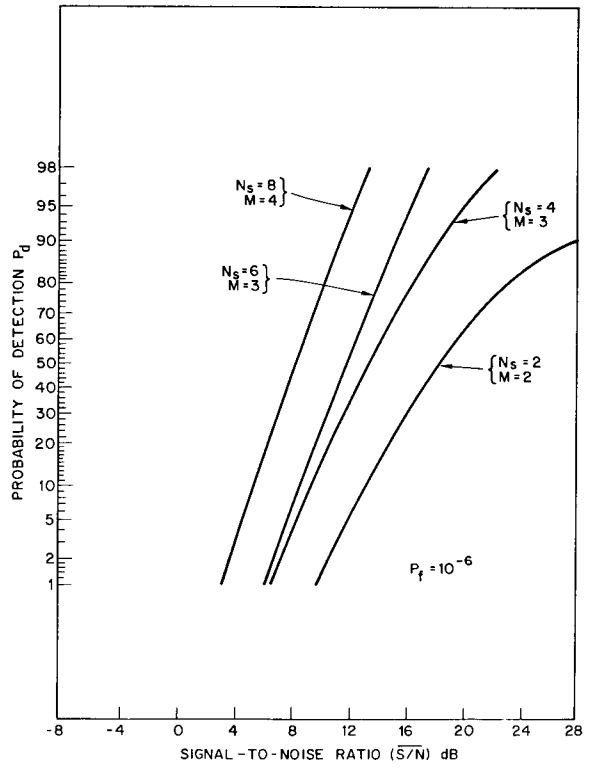

Fig. 38 — Probability of detection vs S/N for $\rho = 0.1$ and $(\overline{S/N}) = 10$ dB (linear minus largest integrator)

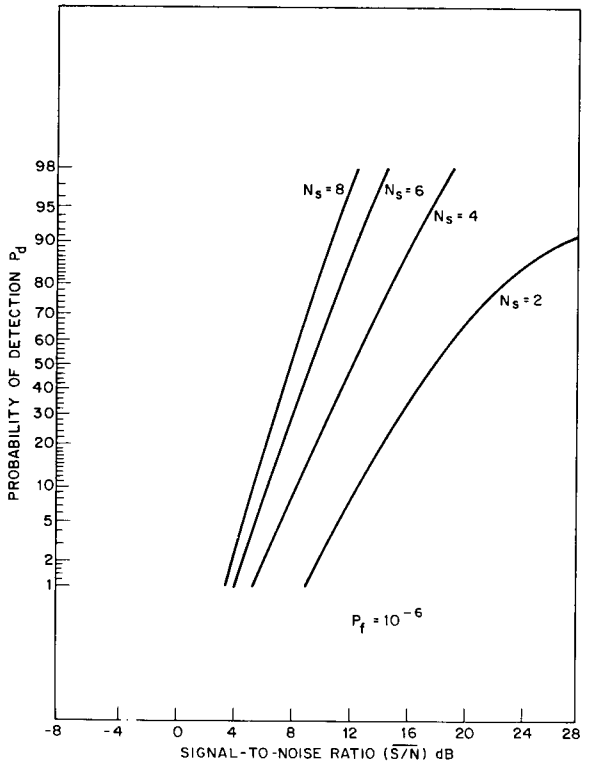

Fig. 39 — Probability of detection vs S/N for $\rho = 0.1$ and $(\overline{S/N}) = 10$ dB ($M + 1$ binary integrator)

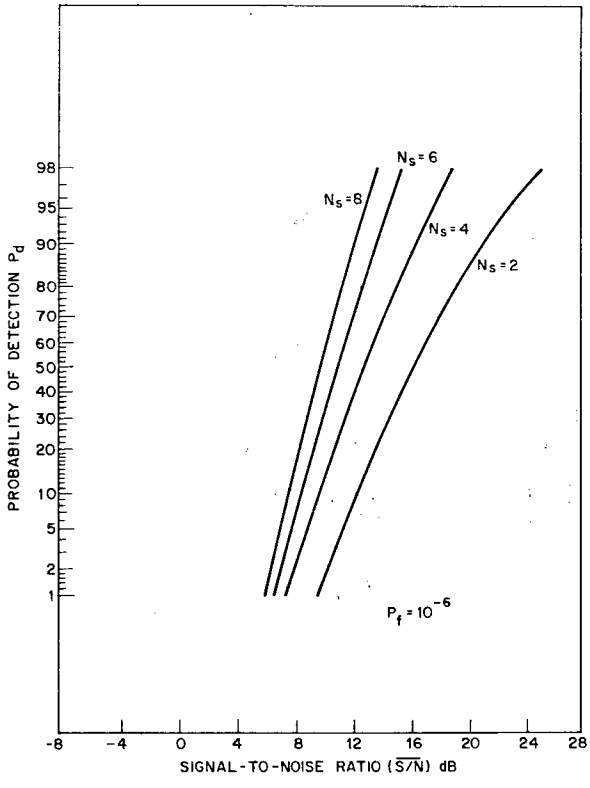

Fig. 40 — Probability of detection vs S/N for $\rho = 0.01$ and $(\overline{S/N}) = 10$ dB (square law integrator)

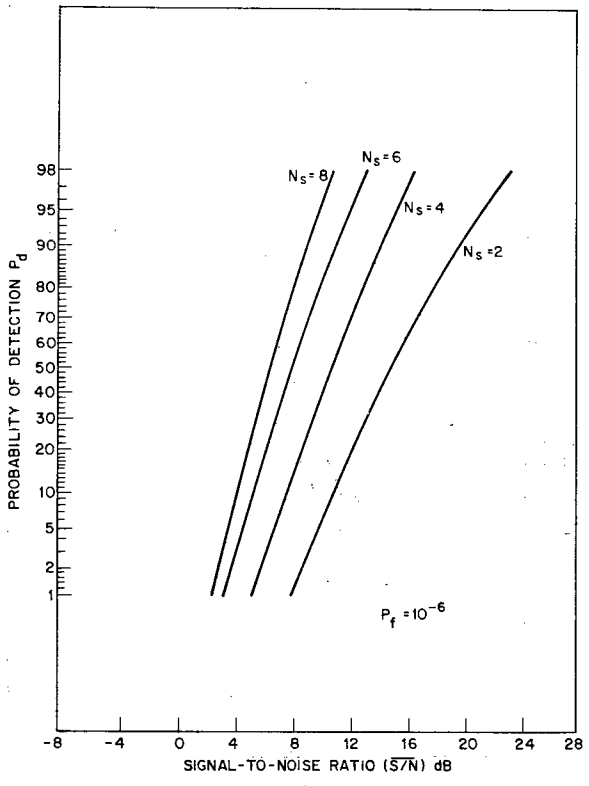

Fig. 41 — Probability of detection vs S/N for $\rho = 0.01$ and $(\overline{S/N}) = 10$ dB (linear integrator)

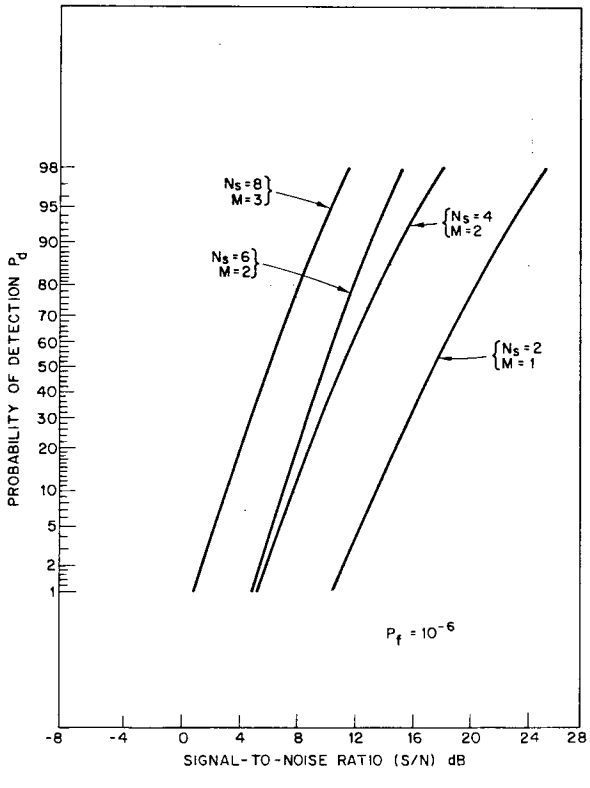

Fig. 42 — Probability of detection vs S/N for $\rho = 0.01$ and $(\overline{S/N}) = 10$ dB (binary integrator)

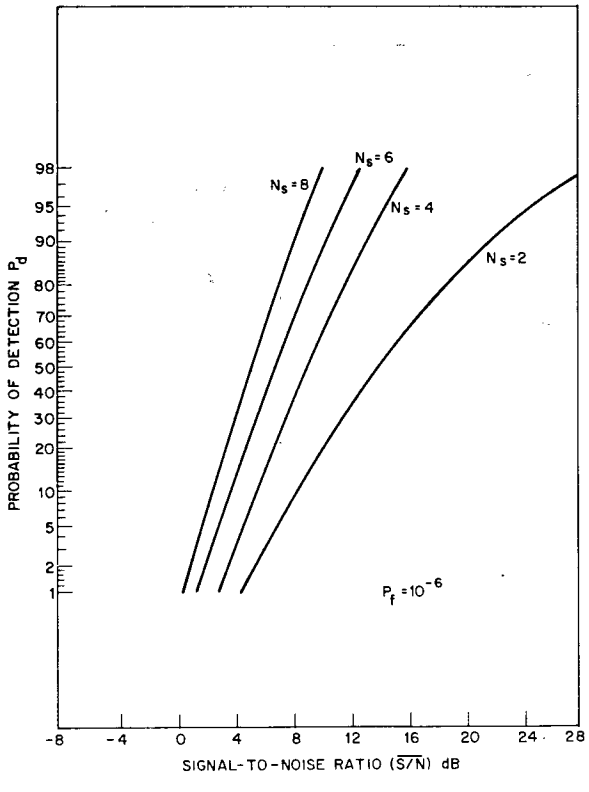

Fig. 43 — Probability of detection vs S/N for $\rho = 0.01$ and $(\overline{S/N}) = 10$ dB (square law minus largest integrator)

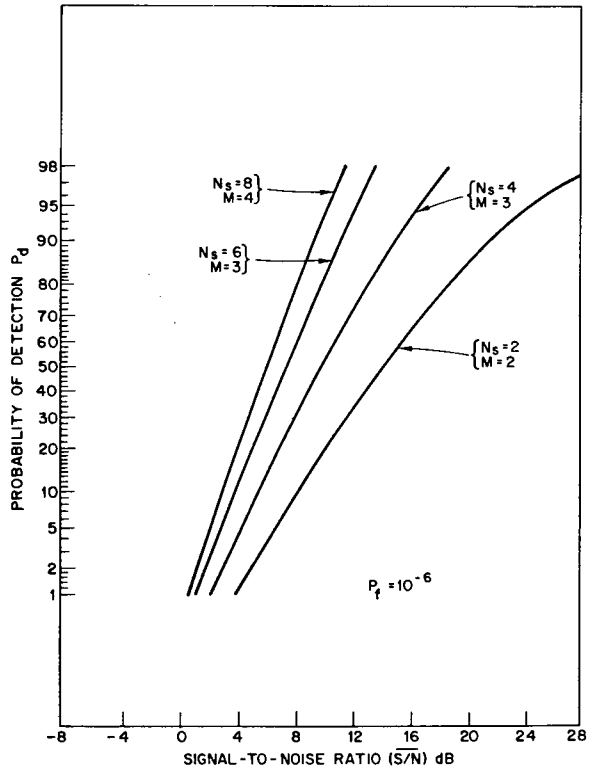

Fig. 44 — Probability of detection vs S/N for $\rho = 0.01$ and $(\overline{S/N}) = 10$ dB (linear-largest integrator)

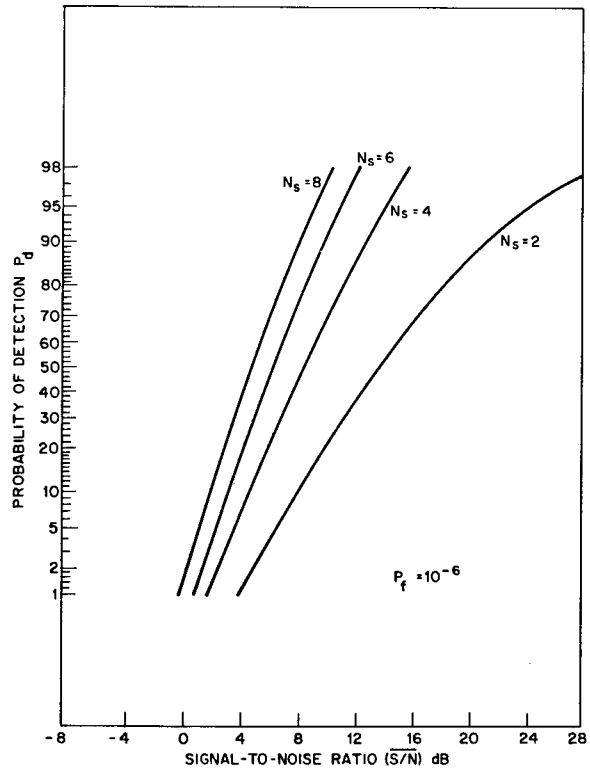

Fig. 45 — Probability of detection vs S/N for $\rho = 0.01$ and $(\overline{S/N}) = 10$ dB ($M + 1$ binary integrator)

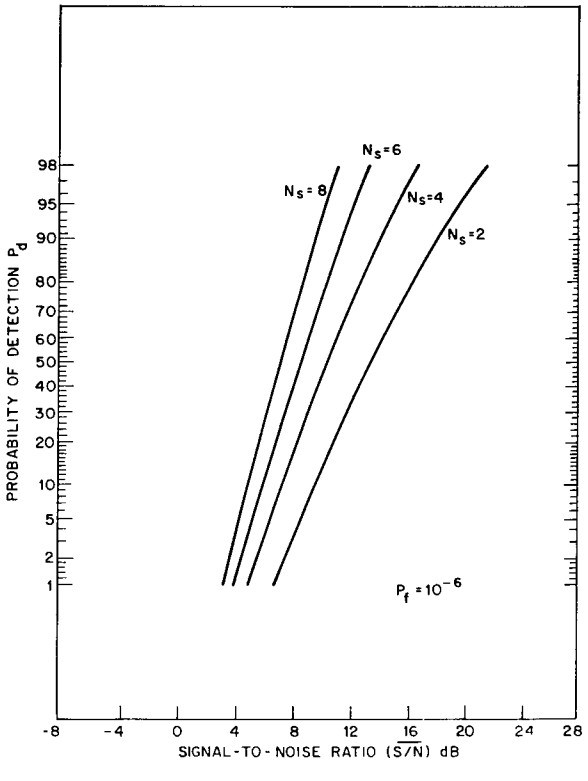

Fig. 46 — Probability of detection vs S/N for $\rho = 0.1$ and $(\overline{S/N}) = 3$ dB (square law integrator)

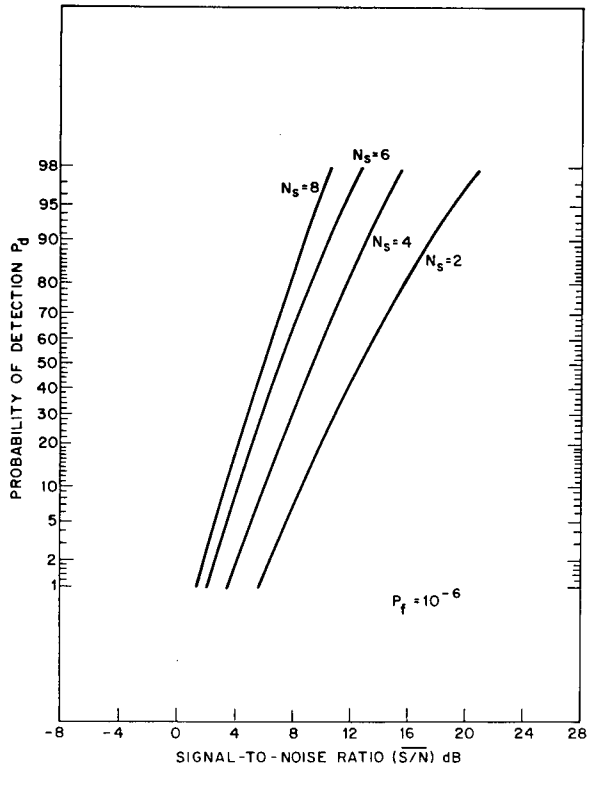

Fig. 47 — Probability of detection vs S/N for $\rho = 0.1$ and $(\overline{S/N}) = 3$ dB (linear integrator)

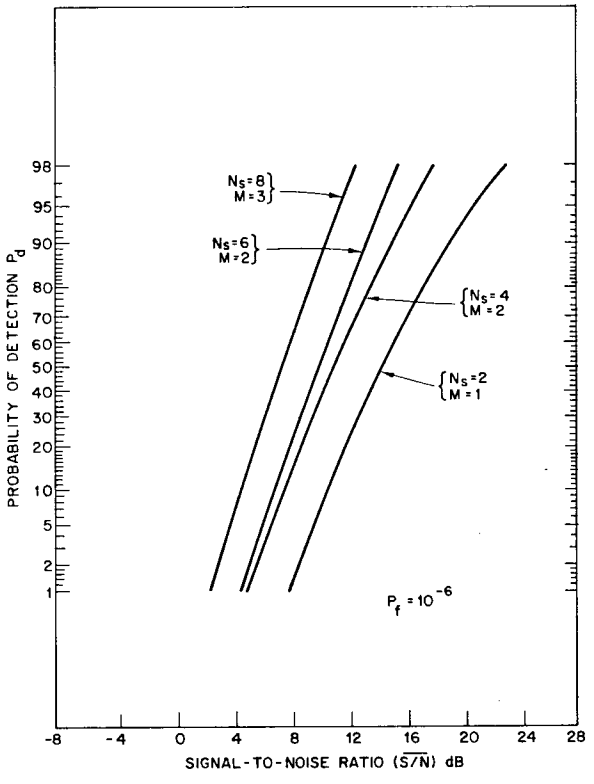

Fig. 48 — Probability of detection vs S/N for $\rho = 0.1$ and $(\overline{S/N}) = 3$ dB (binary integrator)

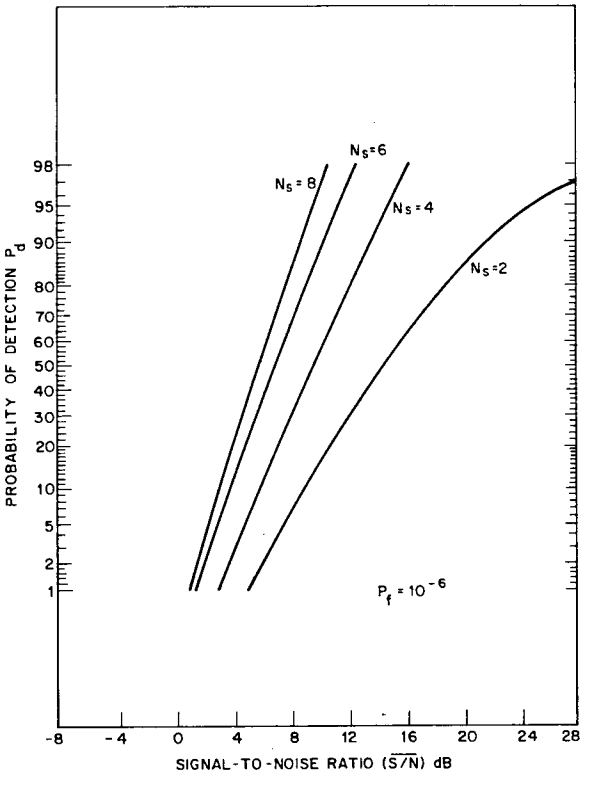

Fig. 49 — Probability of detection vs S/N for $\rho = 0.1$ and $(\overline{S/N}) = 3$ dB (square law minus largest integrator)

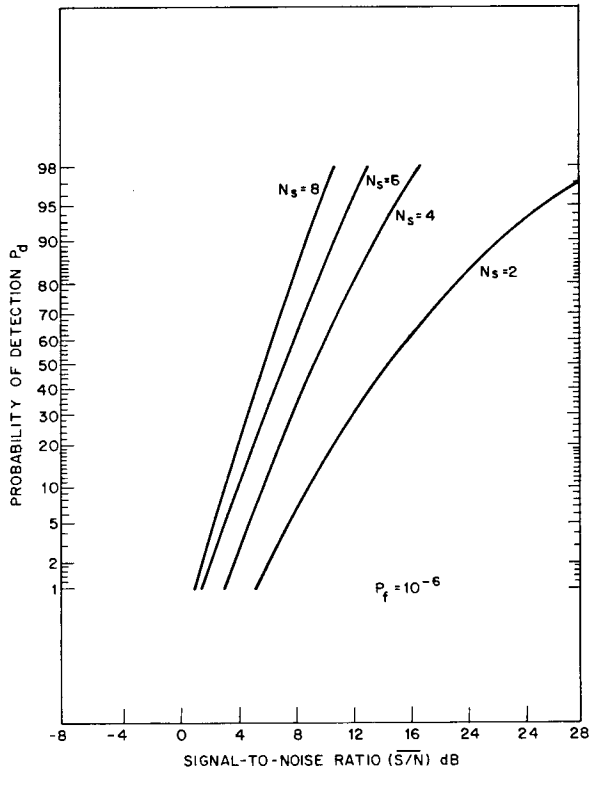

Fig. 50 — Probability of detection vs S/N for $\rho = 0.1$ and $(\overline{S/N}) = 3$ dB (linear minus largest integrator)

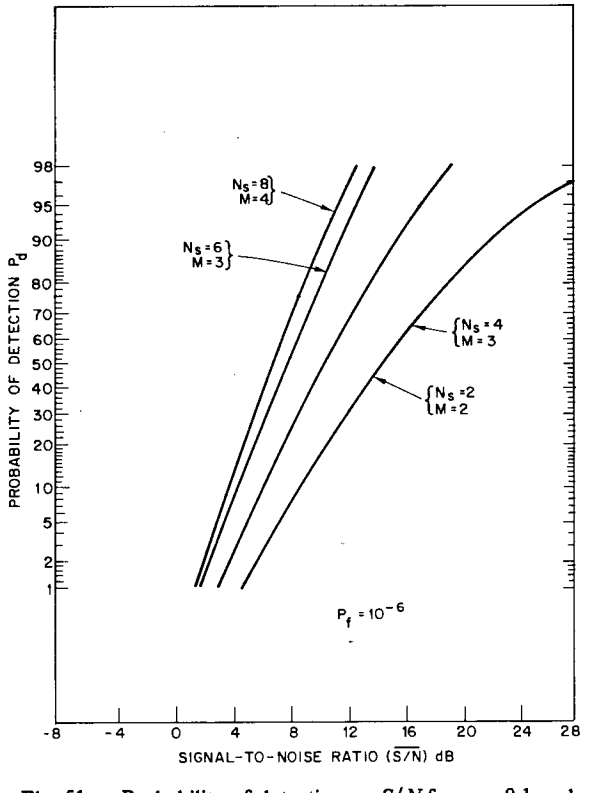

Fig. 51 — Probability of detection vs S/N for $\rho = 0.1$ and $(\overline{S/N}) = 3$ dB ($M + 1$ binary integrator)

COMPARISON OF INTEGRATORS

S/N Improvement

We compare the integrators on the basis of signal-to-noise improvement on multiple dwells with respect to the S/N required to detect a target on a single dwell using a square law and/or linear detector for a fixed probability of false detection P_f and probability of detection P_d. The results for a $P_f = 10^{-6}$ and $P_d = 0.5$ are shown in Figs. 52 to 55, and the results for a $P_f = 10^{-6}$ and $P_d = 0.9$ are shown in Figs. 56 to 59. The background conditions for each figure as to the target density and average S/N of the background are listed on the figures.

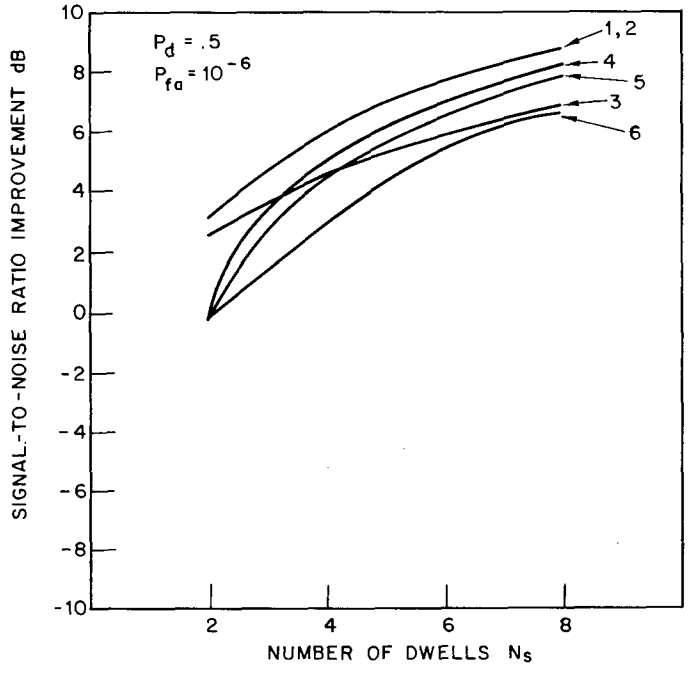

Fig. 52 — Comparison of six integrators on the basis of S/N-improvement vs number of dwells given noise background, $P_f = 10^{-6}$, and $P_d = 0.5$

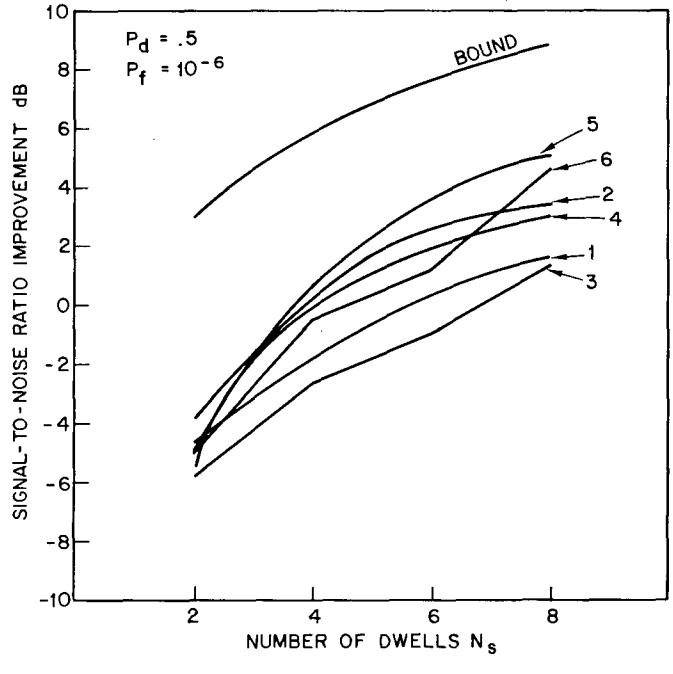

Fig. 53 — Comparison of six integrators on the basis of S/N-improvement vs number of dwells given $\rho = 0.1$, $(\overline{S/N}) = 10$ dB, $P_f = 10^{-6}$, and $P_d = 0.5$

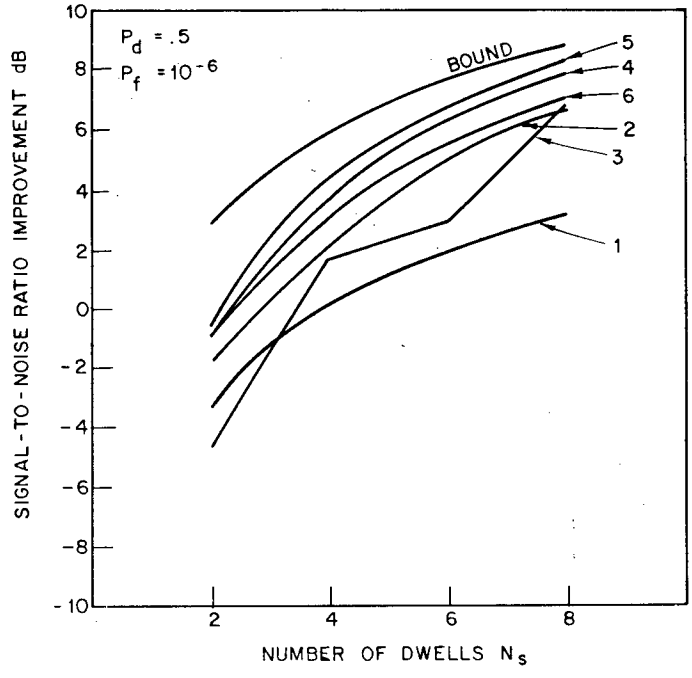

Fig. 54 — Comparison of six integrators on the basis of S/N-improvement vs number of dwells given $\rho = 0.01$, $(\overline{S/N}) = 10$ dB, $P_f = 10^{-6}$, and $P_d = 0.5$

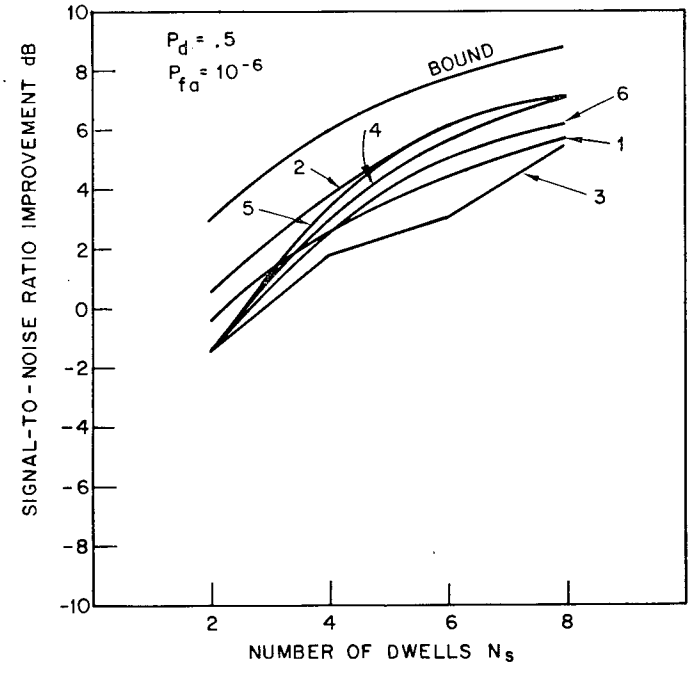

Fig. 55 — Comparison of six integrators on the basis of S/N-improvement vs number of dwells given $\rho = 0.1$, $(\overline{S/N}) = 3$ dB, $P_f = 10^{-6}$, and $P_d = 0.5$

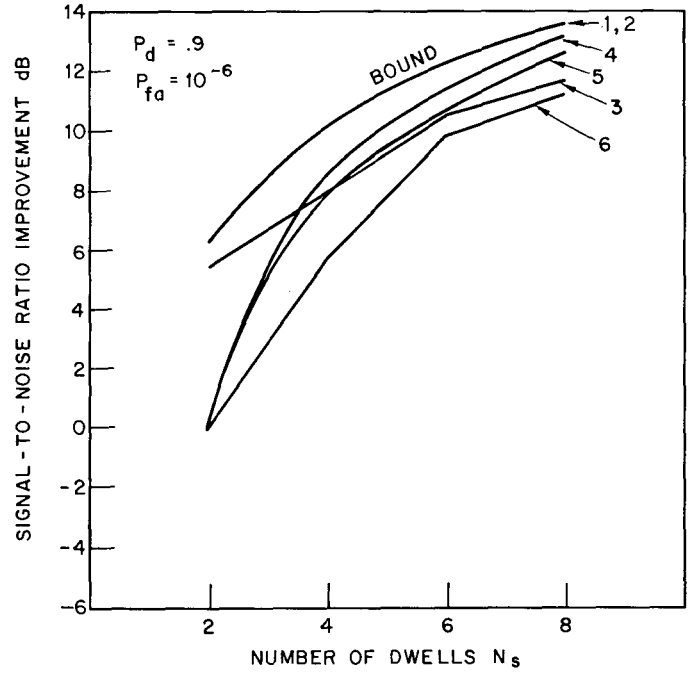

Fig. 56 — Comparison of six integrators on the basis of S/N-improvement vs number of dwells given noise background, $P_f = 10^{-6}$, and $P_d = 0.9$

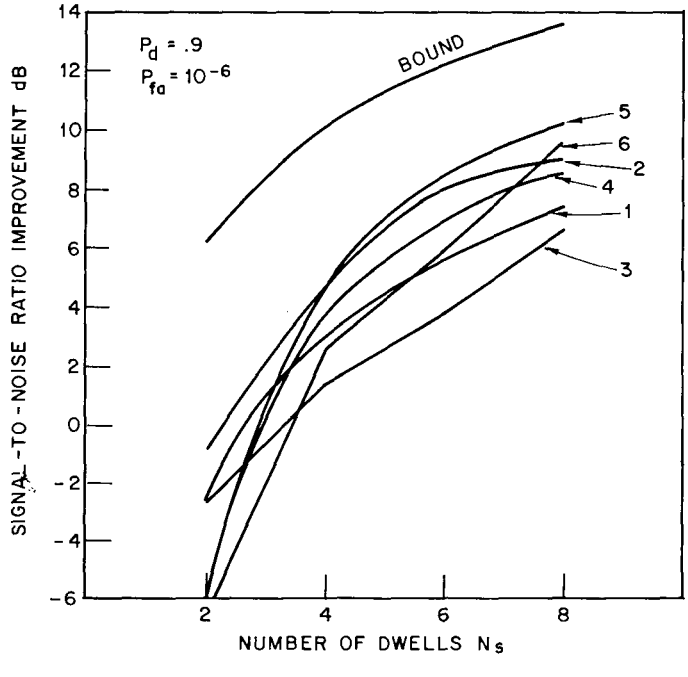

Fig. 57 — Comparison of six integrators on the basis of S/N-improvement vs number of dwells given $\rho = 0.1$, $(\overline{S/N}) = 10$ dB, $P_f = 10^{-6}$, and $P_d = 0.9$

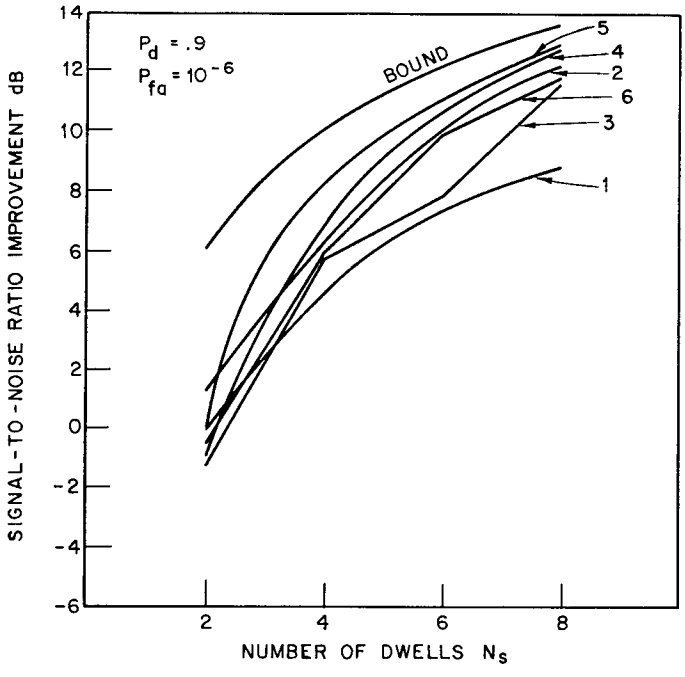

Fig. 58 — Comparison of six integrators on the basis of S/N-improvement vs number of dwells given $\rho = 0.01$, $(\overline{S/N}) = 10$ dB, $P_f = 10^{-6}$, and $P_d = 0.9$

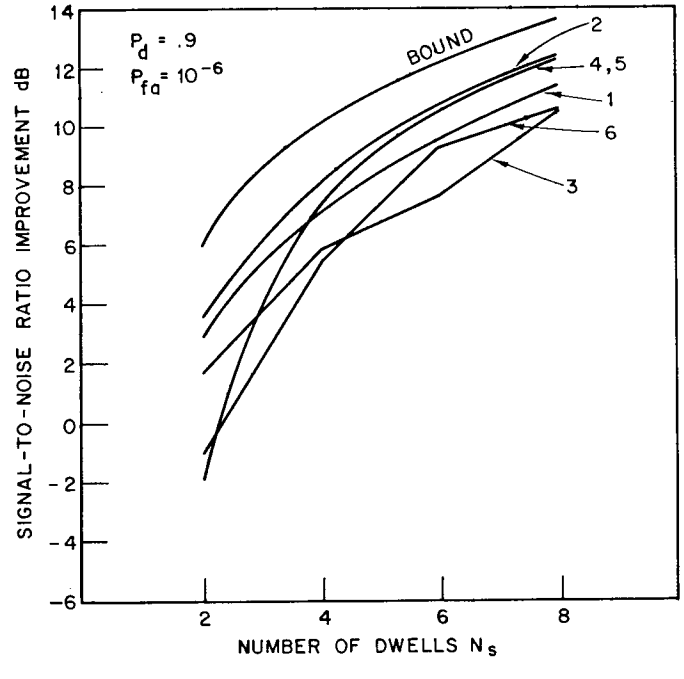

Fig. 59 — Comparison of six integrators on the basis of S/N-improvement vs number of dwells given $\rho = 0.1$, $(\overline{S/N}) = 3$ dB, $P_f = 10^{-6}$, and $P_d = 0.9$

Observing Figs. 52 and 56, the case of no other background targets, we find the one square law, two linear, and three binary integrators obtain the same signal-to-noise improvement with the dwells integrated as the standard noncoherent integration. This improvement can be quite significant. Consequently, the results for the square law and linear integrators, with no other background targets, represents an upper bound in performance and are shown as reference in the other curves. We note that there is little loss in performance when the largest sample is removed or when we require $M + 1$ threshold crossings in the binary integrator as compared to each of the standard integrators.

We make these general observations (Figs. 53 to 59) when there is a background of targets: (a) the square law is generally worse than the linear integrator; (b) the square law minus the largest sample is worse than linear minus the largest sample; (c) and when the targets are strong and dense, the integrators which remove the largest signal or require an additional intermediate detection perform better than the standard integrators. The reasons for these results are: (a) an extraneous strong signal in the linear integrator does not have the impact on the false detection rate and required threshold as the square of the strong signal and, consequently, the linear detector performs best; and (b) the integrators which remove the strongest extraneous signals perform better than the standard integrators in a dense strong target environment because these thresholds can be lower. Using these conclusions, we will only consider further the two most promising integrators: the linear minus the largest sample and $M + 1$ binary integrator.

For the linear-minus-the-largest integrator, the S/N vs the number of dwells for a probability of false alarm $P_f = 10^{-6}$ is given in Fig. 60 for a $P_d = 0.5$ and Fig. 61 for a $P_d = 0.9$. Similarly, for the $M + 1$ binary integrator, the S/N vs the number of dwells for a probability of false alarm $P_f = 10^{-6}$ is given in Fig. 62 for a $P_d = 0.5$ and Fig. 63 for a $P_d = 0.9$.

From Figs. 60 to 63 we note: (a) The medium target density $\rho = 0.01$ and no background target cases yielded nearly the same detection results. (b) We take an increasingly larger loss with increasing target strength and target density because more than one extraneous strong target signal will be in an integrator; this would cause a ghost detection if the threshold were not raised. (c) The linear minus the largest sample is slightly better than the $(M + 1)$ binary detector for the cases studied.

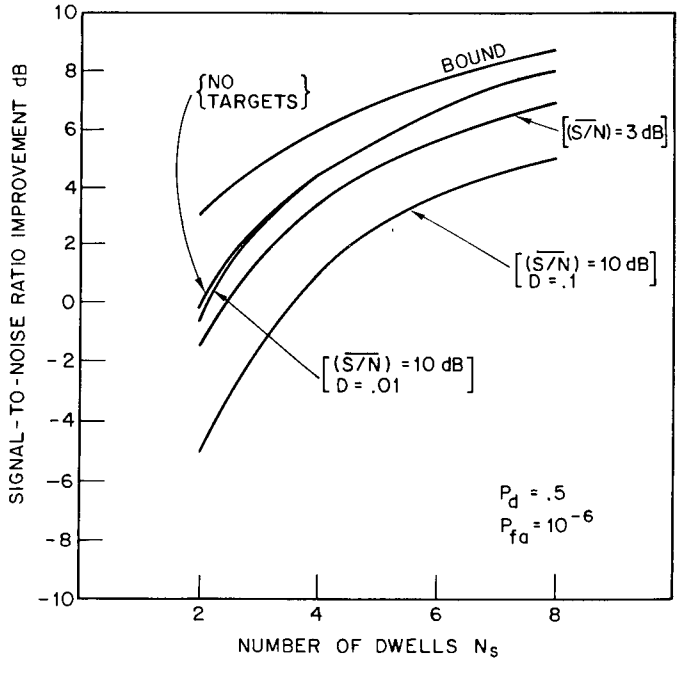

Fig. 60 — Comparison of the linear minus the largest integrator on the basis of S/N-improvement vs number of dwells for a number of target background conditions, $P_f = 10^{-6}$, and $P_d = 0.5$

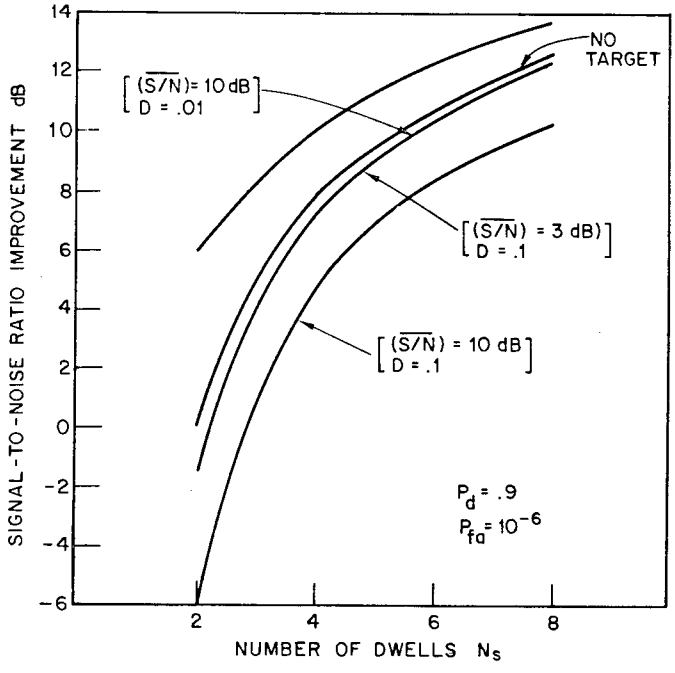

Fig. 61 — Comparison of the linear minus the largest integrator on the basis of S/N-improvement vs number of dwells for a number of target background conditions, $P_f = 10^{-6}$, and $P_d = 0.9$

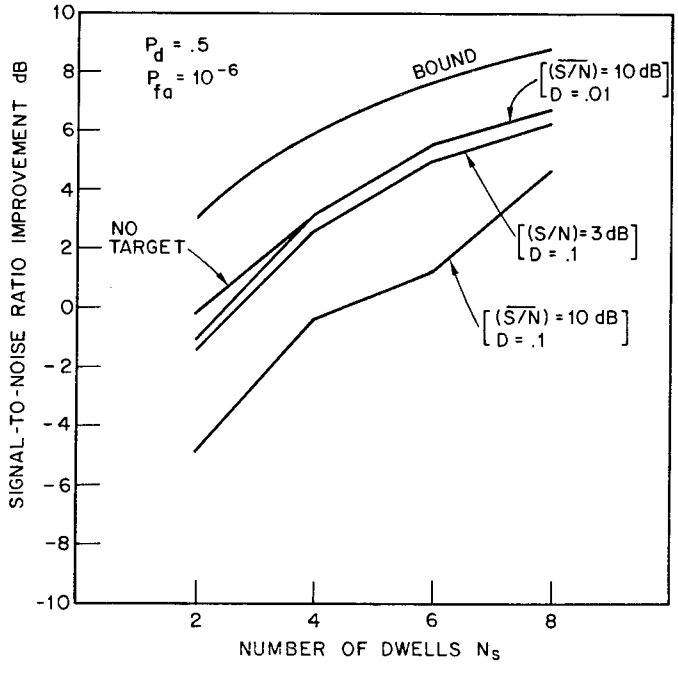

Fig. 62 — Comparison of the $(M + 1)$ binary integrator on the basis of S/N-improvement vs number of dwells for a number of target background conditions, $P_f = 10^{-6}$, and $P_d = 0.5$

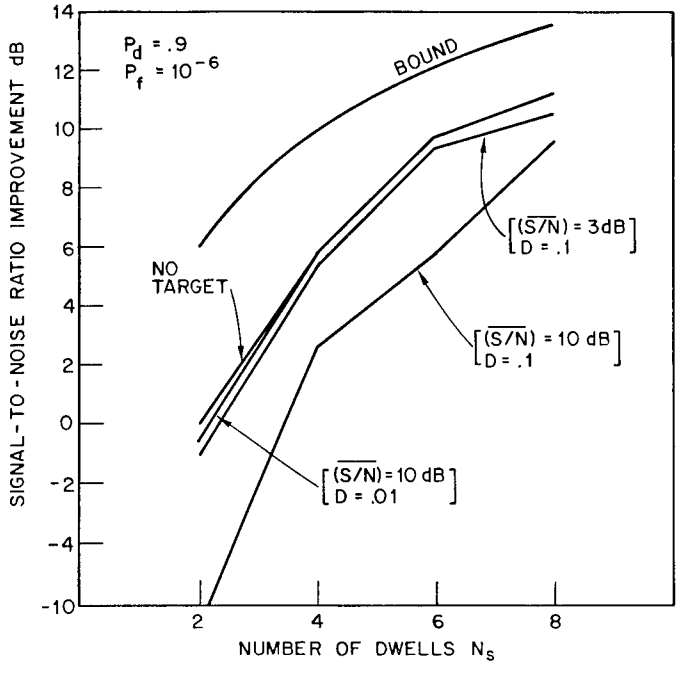

Fig. 63 — Comparison of the $(M + 1)$ binary integrator on the basis of S/N-improvement vs number of dwells for a number of target background conditions, $P_f = 10^{-6}$, and $P_d = 0.9$

False Detection Control

We compare the probability of false detection of each integrator in a background of targets based on thresholds set for a thermal noise environment. We determine the thresholds for all six integrators that yield a $P_f = 10^{-6}$ when only noise is present. We then determine the probability of false alarm under various backgrounds using these thresholds. The results of this probability of false detection vs dwells are shown in Figs. 64 to 66 where the target background parameters are listed on the figures. We find from these figures that the linear minus the largest sample and $(M + 1)$ binary detectors are best at maintaining lower false detection rates when the thresholds are all set for $P_f = 10^{-6}$ in thermal noise. Observe in the dense environment (see Fig. 64), we obtained 10^{-4} false detection rate even though the thresholds were set for thermal noise.

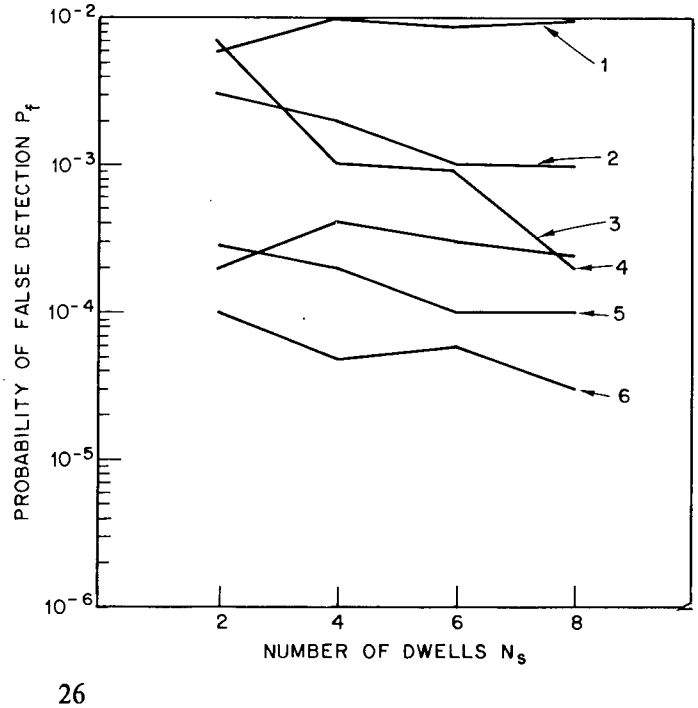

Fig. 64 — Probability of false detection for the six integrators vs number of dwells using a noise only background threshold set for $P_f = 10^{-6}$ for a $\rho = 0.1$ and $(\overline{S/N})$ = 10 dB target background

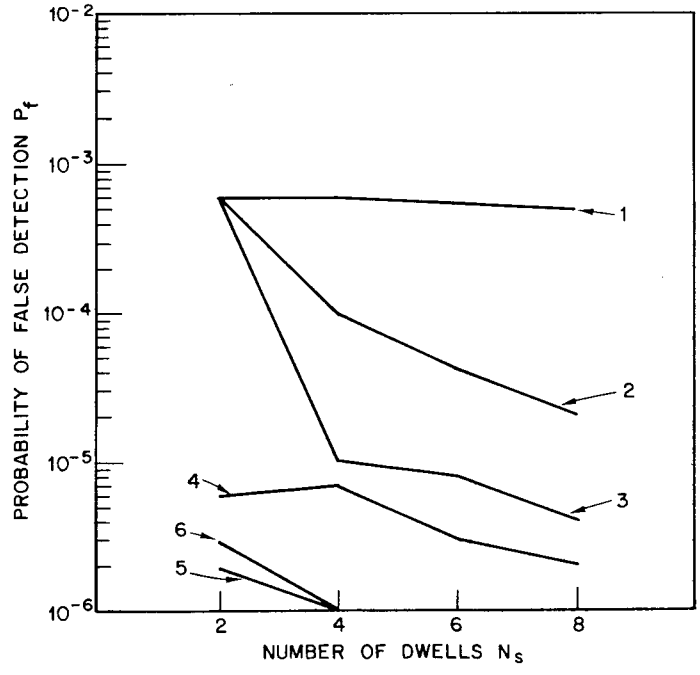

Fig. 65 — Probability of false detection for the six integrators vs number of dwells using a noise only background threshold set for $P_f = 10^{-6}$ for a $\rho = 0.01$ and $(\overline{S/N}) = 10$ dB target background

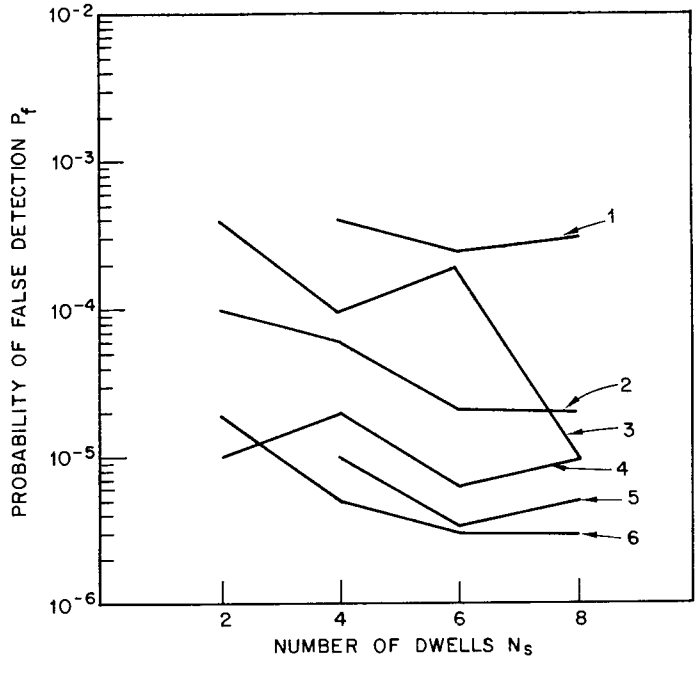

Fig. 66 — Probability of false detection for the six integrators vs number of dwells using a noise only background threshold set for $P_f = 10^{-6}$ for a $\rho = 0.1$ and $(\overline{S/N}) = 3$ dB target background

Discussion

We have found that the linear minus the largest sample and the $(M + 1)$ binary integrator did a credible job of controlling the false detection rate with a fixed threshold even in a dense, *fairly-strong-target* environment. Furthermore, we found that these integrators yielded probability of detections which were near the upper bound. The reason these integrators performed well is that they controlled the ghost target detection which were primarily obtained from a single target signal located in an integrator that does not contain a target. The threshold did not have to be raised significantly to control the false detections because the signals which would cause the false detection had been thrown out. Consequently, since the threshold is nearly the same whether there are many targets or not, the probability of detection is near the upper bound.

The preceding discussion suggests two mechanisms for controlling the false detection rate. First, by controlling the threshold, the second by requiring an integrator defined by either removing a few of the largest samples from the linear integrator or by requiring a few more intermediate detections in the binary integrator. The number of large samples removed from the linear integrator would depend on the target density. For example, in a light target environment only the largest sample would be removed, and in a heavy environment, possibly several of the largest samples would be removed. Since it is the ghost targets which make up the false detections in dense environments, removing several of the larger samples would not allow a ghost target to be formed from signals from several targets. The fewer number of large samples removed the smaller the detection loss. Similar operations could be performed on the binary integrator.

A significant by-product benefit of the process is that velocity as well as location is obtained. If the radar were sensitive so that it could detect birds and insects, the high-speed aircraft can be separated easily from these other objects on the basis of velocity.

The results given in this report illustrate that detection improvement can be achieved for a number of cases and that it was usually advantageous to exclude the largest sample. This was particularly true in dense environments. Of course, the results are a function of the statistics and will vary somewhat depending on the environment. Although it was virtually impossible to include a wide variety of cases in the simulation, the cases run were representative of the performance one would expect.

SUMMARY

Six long-term radar integrators which accounted for target motion were studied under the conditions of a set of background targets. For the conditions studied, excellent false-alarm control and detection improvement near the bounds for noise conditions could be obtained with the linear-minus the largest sample and $(M + 1)$ binary integrators. The reason for this result is that ghost targets can appear and these integrators eliminated them with little loss in detection of *true* targets. The ghost targets are caused by a few (usually one but can be a few) real signals located in integrators which do not contain real targets. By eliminating a few (one often is sufficient) of the larger signals or requiring extra intermediate detections in the binary integrator, most ghost targets are suppressed. We hypothesize that adaptive false-alarm control would involve both the threshold adjustment as well as the number of larger signals removed in a linear integrator or number of additional intermediate detections required in a binary integrator as a function of target density. Finally, since velocity is a by-product of the integration, low-speed targets such as birds and insects, etc., can be separated from high-speed air targets.

REFERENCES

1. M.I. Skolnik, ed., *Radar Handbook*, McGraw-Hill Book Co., 1970.

2. R.J. Prengaman, R.E. Thurber, and W.G. Bath, "A Retrospective Detection Algorithm for Extraction of Weak Targets in Clutter and Interference Environments," *International Conference RADAR-82, IEE Conference* Publication Number 216, Oct. 1982, 18-20 p. 341.

3. G.J. Linde and W.M. Waters, "An Interleaved-Trace Time-Compression Radar Display," *IEEE Trans. Aerospace and Electric Systems,* AES-17 Sept. 1981, pp. 724-726.

4. B.H. Cantrell and G.V. Trunk, "Correction to Angular Accuracy of a Scanning Radar Employing a Two-Pole Filter," *IEEE Trans. Aerospace and Electronic Systems*, AES-10 Nov. 1974, pp. 878-880.

5. R.L. Mitchell, "Importance Sampling Applied to Simulation of False Alarm Statistics," *IEEE Trans. Aerospace and Electronic Systems*, AES-17 Jan. 1981, pp. 15-21.

6. J. Pachares, "A Table of Bias Levels Useful in Radar Detection Problems," *IRE Trans. Information Theory,* IT-4 Mar. 1958, pp. 38-45.

7. G.H. Robertson, "Operating Characteristics for a Linear Detector of CW Signals in Narrow-Band Gaussian Noise," *Bell Syst. Tech. J. 46*, April 1967, pp. 755-774.

8. R. Worley, "Optimum Thresholds for Binary Integration," *IEEE Trans. Information Theory,* IT-14 Mar. 1968, pp. 349-353.